IWS1 phosphorylation by AKT3 controls nuclear export of type I IFN mRNAs and sensitivity to oncolytic viral infection, by regulating the alternative RNA splicing of *U2AF2.*

Georgios I. Laliotis[1,2,3,12*], Adam D. Kenney[4,5], Evangelia Chavdoula[1,2] , Arturo Orlacchio[1,2], Abdul K. Kaba[1,2], Alessandro La Ferlita[1,2,6], Vollter Anastas[1,2,7], Christos Tsatsanis[8,9], Joal D. Beane[2,10], Lalit Sehgal[11], Vincenzo Coppola[1,2] , Jacob S. Yount [4,5] and Philip N. Tsichlis[1,2,13*]

[1]The Ohio State University, Department of Cancer Biology and Genetics, Columbus, OH, 43210, [2]The Ohio State University Comprehensive Cancer Center-Arthur G. James Cancer Hospital and Richard J. Solove Research Institute, Columbus, OH, 43210, [3]University of Crete, School of Medicine, Heraklion Crete, 71500, Greece, [4]Department of Microbial Infection and Immunity, The Ohio State University, Columbus, OH, 43210, [5]Infectious Diseases Institute, The Ohio State University, Columbus, OH, 43210, [6]Department of Clinical and Experimental Medicine, Bioinformatics Unit, University of Catania, Catania, 95131, Italy, [7]Tufts Graduate School of Biomedical Sciences, Program in Genetics, Boston, MA, 02111 [8]Department of Clinical Chemistry-Biochemistry, School of Medicine, University of Crete, Heraklion 71110, Crete, Greece, [9]Institute for Molecular Biology and Biotechnology, Foundation for Research and Technology Hellas, Heraklion 70013, Greece, [10]The Ohio State University, Department of Surgery, Division of Surgical Oncology, Columbus, OH 43210 [11]College of Medicine, Department of Hematology, The Ohio State University, Columbus, OH 43210

Present Address :

[12]The Sidney Kimmel Comprehensive Cancer Center, Johns Hopkins University, Baltimore, MD, 21231

Running Title: IWS1 affects sensitivity to oncolytic viruses

[13]Lead Contact

*Correspondence should be addressed to: Philip N. Tsichlis (Philip.tsichlis@osumc.edu) and Georgios I. Laliotis (glaliot7@gmail.com)

Abstract

Type I IFNs orchestrate the antiviral response. Interestingly, *IFNA1* and *IFNB1* genes are naturally intronless. Based on previous work, the splicing factor U2 Associated Factor 65 (U2AF65), encoded by *U2AF2*, and pre-mRNA Processing factor 19 (Prp19) function on the Cytoplasmic Accumulation Region Elements (CAR-E), affecting the nuclear export of intronless genes. We have previously shown that the loss of IWS1 phosphorylation by AKT3, promotes the alternative RNA splicing of *U2AF2*, resulting in novel transcripts lacking exon 2. This exon encodes part of the Serine-Rich (RS) domain of U2AF65, which is responsible for its binding with Prp19. Here, we show that IWS1 phosphorylation and the *U2AF2* RNA splicing pattern affect the nuclear export of introless mRNAs. We also demonstrate that the same axis is required for the proper function of the CAR-Es. Mechanistically, whereas both U2AF65 isoforms bind CAR-E, the recruitment of Prp19 occurs only in cells expressing phosphorylated IWS1, promoting intronless genes export. Moreover, analysis of Lung adenocarcinoma patients showed that high p-IWS1 activity correlates with the assembly of the U2AF65/Prp19 complex and export of intronless genes, *in vivo*. Accordingly, the expression of type I IFNs was decreased in cells deficient in IWS1 phosphorylation and the viral infection was increased. Furthermore, following infection with oncolytic virus, we observed reduced activation of p-STAT1 and expression of Interferon Stimulated Genes (ISG), in cells stimulated by shIWS1-derived supernatant, or cells treated with the pan-AKT inhibitor, MK2206. Consistently, killing curves and apoptosis assays after infection with oncolytic viruses, revealed increased susceptibility upon the loss of IWS1, with subsequent activation of Caspase-mediated death. The treatment of the lung adenocarcinoma cells with MK2206, phenocopied the loss of IWS1 phosphorylation. These data identify a novel mechanism by which the AKT/p-IWS1 axis, by hijacking the epigenetic regulation of RNA splicing and processing, contributes to the resistance to oncolytic viral infection, suggesting that combined inhibition of the splicing machinery and AKT/p-IWS1 signals would sensitize tumors to oncolytic viral treatment.

58 **Introduction**

59 Type I interferons (IFNs) are members of a large signaling family of proteins, known
60 for their robust antiviral response. Specifically, type I IFNs are encoded by 13 *IFNA* genes and
61 a single *IFNB* gene (Frisch et al., 2020[1]). These genes are rapidly induced by Pattern
62 Recognition Receptors (PRRs), the sensors of innate immunity (Acosta et al., 2020[2]). These
63 receptors recognize molecules presented by pathogens (pathogen-associated molecular
64 patterns, PAMPs), such as double-stranded RNA (dsRNA), bacterial lipopolysaccharides,
65 flagellin, bacterial lipoproteins, and cytosolic DNA. (Amarante-Mendes et al., 2018[3]). Signals
66 from PRRs converge upon IKK-family kinases to phosphorylate and activate two transcription
67 factors, IRF3 and NF-kB; these factors directly transactivate the *IFNB1* gene (Ablasser et al.,
68 2020[4]). IFNβ in an autocrine or paracrine manner and activates the IFNAR1/2 receptors,
69 resulting in Janus kinase (JAK)-mediated phosphorylation of STAT1 and STAT2, forming a
70 canonical complex of STAT1/STAT2/IRF9, known as the Interferon Stimulated Gene Factor 3
71 (ISGF3) complex. This activated complex transcribes target genes (interferon-stimulated
72 genes, ISGs) containing ISRE (ISGF3 response elements), that limit viral replication (Aleynick
73 et al., 2019[5]).

74 Activation of the type I IFN pathway is critical in antiviral immunity and in mediating a
75 wide array of innate immune responses. Modulating this pathway is not only critical for
76 controlling antiviral and inflammatory responses, but it also offers translational applications.
77 One of the most important translational applications of the activation of this pathway is the
78 usage of oncolytic viruses (OV). OVs have gained momentum in recent years because of their
79 immune-stimulating effects, both systemically and in the local tumor microenvironment (Park
80 et al., 2020[7]). The first clinically approved OV, Talimogene laherparepvec (TVEC), is a
81 genetically modified type I herpes simplex virus (HSV) that expresses granulocyte-
82 macrophage colony-stimulating factor (GM-CSF) (Rehman et al., 2016[7]). While TVEC is
83 routinely used in select patients with melanoma, most other OVs have not shown robust
84 antitumor efficacy in clinical trials, especially when used as monotherapy (Martinez-Quintanilla

85 et al., 2019[8]). Thus, deeper comprehension of the molecular pathways involved in the efficacy
86 of these therapeutic approaches is a necessity for the proper design of antitumor oncolytic
87 therapies.

88 One way to improve the response to OV therapy is through the manipulation of multiple
89 signalling pathways regulating the type I IFN response. Among them, the AKT pathway
90 regulates the IFN response at multiple levels, with many of its activities being isoform-specific.
91 Early studies have shown that by activating the mechanistic target of rapamycin (mTOR), AKT
92 promotes the translation of ISGs (Kroczynska et al., 2014[9]). Subsequent studies revealed that
93 AKT1 activates β-catenin, promoting the transcriptional activation of *IFNB1* (Gantneret al.,
94 2012[10]). In addition, we have shown that AKT1 selectively phosphorylates EMSY at S209,
95 relieving the EMSY-mediated repression of ISGs (Ezell et al., 2012[11]).

96 Interestingly, genes encoding *IFNA1* and *IFNB1* are naturally intronless (de Padilla et
97 al., 2014[12]). In contrast to splicing-dependent mRNA export, little is known regarding the
98 nuclear export of intronless mRNAs. Based on previous reports, components of the
99 Transcription-Export (TREX) complex, the pre-mRNA Processing Factor 19 (Prp19) complex
100 and the splicing factor U2 Associated-Factor 2 (U2AF2) associate with designated
101 Cytoplasmic Accumulation Region Elements (CAR-E), a 10-nt consensus element on
102 intronless genes, and function in their mRNA export (Lei et al., 2013[13]). These data suggest
103 the presence of an additional layer in the regulation of type I IFN expression.

104 Based on our previous observations, IWS1 (Interacts With Spt6) is an RNA processing
105 factor and phosphorylation target of AKT kinase at S720/T721 (Sanidas et al., 2014[14]). More
106 recently we revealed that IWS1 phosphorylation affects genome-wide the alternative RNA
107 splicing program in human lung adenocarcinoma (Laliotis et al., 2020[15]). In one example, the
108 loss of phosphorylated IWS1 resulted in a novel, exon 2 deficient splice variant of the splicing
109 factor *U2AF2.* This exon encodes part of the U2AF65 Serine-Rich (RS) Domain, which is
110 required for its binding with Prp19, further affecting the downstream splicing machinery. We
111 also provided evidence that the *U2AF2* exon 2 inclusion depends on phosphorylated IWS1,

112 by promoting histone H3K36 trimethylation by SETD2 and the assembly of LEDGF/SRSF1
113 splicing complexes, in a cell-cycle specific manner (Laliotis et al., 2020[16]).

114 Since IWS1 phosphorylation controls the U2AF65-Prp19 interaction through the
115 epigenetic regulation of *U2AF2* alternative RNA splicing, we sought to investigate the effect of
116 this pathway in the nucleocytoplasmic export of naturally intronless genes, including *IFNA1*
117 and *IFNB1.* In this study, our goal was to elucidate the molecular mechanisms, following IWS1
118 phosphorylation and the subsequent hijacking of alternative RNA splicing program, that affect
119 the nucleocytoplasmic export of intronless mRNAs and to highlight a novel role of AKT kinase
120 signaling in the regulation of type I IFN response and sensitivity of lung adenocarcinoma cells
121 to infection with oncolytic viral strains.

122 **Results**

123 **IWS1 phosphorylation regulates the nucleocytoplasmic transport of intronless gene**
124 **mRNAs, via *U2AF2* alternative RNA splicing.**

125 Our earlier studies have shown that the knockdown of IWS1 and its replacement by
126 the non-phosphorylatable mutant IWS1 S720A/T721A, altered the RNA splicing pattern of
127 *U2AF2* (Laliotis et al., 2020[15]). The predominant novel splice variant of the *U2AF2* mRNA that
128 we identified in these cells, lacks exon 2, which encodes part of the N-terminal RS domain of
129 U2AF65. This domain is responsible for the interaction of U2AF65 with Prp19, a component
130 of the seven-member ubiquitin ligase complex Prp19C (Laliotis et al., 2020[15], R. Hogg et al.,
131 2010[17], Chanarat S. et al., 2013[18]). More importantly, U2AF65 and Prp19C, along with
132 components of the TREX complex, bind elements designated as Cytoplasmic Accumulation
133 Region Elements (CAR-E) in naturally intronless mRNAs, promoting their nucleocytoplasmic
134 transport (Lei et al., 2013[13]). Examples of mRNAs whose nucleocytoplasmic transport is
135 regulated by this mechanism include *IFNA1, IFNB1, JUN and HSBP3* (Lei et al., 2013[13]).

136 Based on this knowledge, we hypothesized that IWS1 phosphorylation affects the
137 nucleocytoplasmic export of these mRNAs, through the alternative RNA splicing of *U2AF2*

138 and the U2AF65-Prp19 interaction. First, we engineered shControl, shIWS1, shIWS1/wild type
139 IWS1 rescue (shIWS1/WT-R), shIWS1/phosphorylation site IWS1 mutant rescue
140 (shIWS1/MT-R) and shIWS1/U2AF65α (exon 2-containing) or U2AF65β (exon 2-deficient)
141 rescue NCI-H522 and NCI-H1299 lung adenocarcinoma cells. Notably, the IWS1 rescue
142 clones used are engineered to be shRNA resistant (Sanidas et al., 2014[14]). Subsequently, we
143 confirmed the significant down-regulation of IWS1 expression after the transduction of the
144 cells with a lentiviral shIWS1 construct and the shRNA-resistant rescue of IWS1 knock-down
145 with the Flag-tagged wild type protein and phosphorylation IWS1 site mutant (**Fig. 1A**). In the
146 same cells, we performed RT-PCR investigating the inclusion of *U2AF2* E2. Consistent with
147 our previous results, *U2AF2* exon 2 inclusion occurred in shControl and shIWS1/WT-R cells
148 (**Fig. 1A**) (Laliotis et al., 2020[15]).

149 To further investigate our hypothesis, we fractionated the nuclear and cytosolic
150 compartments of shControl, shIWS1, shIWS1/WT-R, shIWS1/MT-R, shIWS/U2AF65α, and
151 shIWS1/U2AF65β NCI-H522 and NCI-H1299 cell lines, and calculated the Cytoplasmic to
152 Nuclear (C/N) ratio of the set of intronless genes with qRT-PCR. Notably, in order to induce
153 the transcription of type I IFNs (*IFNA1 and IFNB1*), we infected cells with the murine
154 paramyxovirus, Sendai fused with GFP (SeV-GFP), which is a potent and commonly used tool
155 for induction of type I IFNs (Yount et al., 2006[19], Bedsaul et al., 2016[20]). First, using western
156 blotting, we confirmed the validity of the fractionation by the detection of Lamin A/C and
157 GAPDH only in the nuclear and cytosolic protein compartment, respectively (**Fig. S1A**). The
158 results showed decreased Cytosolic/Nuclear ratio in shIWS1 and shIWS1/MT-R, due to
159 nuclear retention of these mRNAs, which was rescued in the shIWS1/WT-R cells. More
160 importantly, consistent with our hypothesis, the ectopic expression of U2AF65α, but not the
161 U2AF65β, rescued the nuclear retention phenotype (**Fig. 1B**).

162 Next, we questioned whether IWS1 also affects the transcription of these intronless
163 genes. To this extent, we examined their total RNA levels using qRT-PCR in shControl,
164 shIWS1, shIWS1/WT-R, shIWS1/MT-R, shIWS1/U2AF65α and shIWS1/U2AF65β NCI-H522

165 and NCI-H1299 cells. Interestingly, we found that the total levels of type I IFN, *JUN* and *HSBP3*
166 were upregulated in the shIWS1 and shIWS1/MT-R cells. Interestingly, the levels of type I IFN,
167 but not *JUN and HSBP3*, were affected by the *U2AF2* RNA splicing pattern (**Fig. 1C**). We
168 interpret these data to suggest that the upregulation of the mRNAs of IFN genes in shIWS1
169 cells may be due to different mechanisms than the upregulation of the mRNAs of other
170 intronless genes. To expand the significance of these observations in human lung
171 adenocarcinoma, analysis of the publicly available data of The Cancer Genome Atlas (TCGA),
172 revealed a negative correlation of *IWS1* levels with the total RNA levels of intronless genes in
173 patients with Lung adenocarcinoma (**Fig. S1B, left panel**). Notably, consistent with the *in vitro*
174 results, analysis of the Reverse Phase Protein Assay (RPPA) in the same patients, revealed
175 a significant positive correlation of p-c-Jun (S73) with p-AKT (S473) levels and the *IWS1* and
176 *AKT3* RNA levels (**Fig. S1B**), further supporting the role of IWS1 in the nucleocytoplasmic
177 export of RNAs transcribed from intronless genes, in human lung adenocarcinoma.

178 Given that only exported mRNAs are translated into protein products, we then
179 examined the protein expression of c-Jun, Hsp27, and IFNβ1 with Western blotting in NCI-
180 H522 and NCI-H1299 cells. Similarly, SeV-GFP infection was performed in order to maximize
181 the type I IFN induction. Consistent with the qRT-PCR data, the results showed reduced
182 expression of the protein products of naturally intronless genes in shIWS1 and shIWS1/MT-R
183 cells, compared to shControl cells, an effect rescued in shIWS1/WT-R. More importantly, the
184 U2AF65α isoform rescues the shIWS1 phenotype, but the U2AF65β did not (**Fig. 1D**). These
185 data support the hypothesis that IWS1 phosphorylation controls the nucleocytoplasmic RNA
186 export transcribed from naturally intronless genes, through a process that depends on *U2AF2*
187 alternative RNA splicing.

188

189 To provide additional support to our model, protein interaction analysis using the
190 STRING database (Szklarczyk et al., 2019[21]) showed the expected interaction of U2AF65 and
191 Prp19 with components of the TREX complex and export machinery, THOC2 and Ref/Aly (**Fig.**

192 **S1C**). Furthermore, analysis of the previously performed RNA-Seq study in NCI-H522
193 shControl, shIWS1, shIWS1/WT-R, and shIWS1/MT-R cells, (Laliotis et al., 2020[15]), using
194 Gene Set Enrichment Analysis (GSEA) (Subramanian et al., 2005[21]), revealed significant
195 enrichment of genes affecting nuclear export in cells expressing phosphorylated IWS1 (**Figure**
196 **S1D**). Taken together, these results support a multi-layered role of IWS1 phosphorylation in
197 the nuclear export machinery.

198 **AKT3 kinase affects the nucleocytoplasmic export of intronless RNAs, through IWS1**
199 **phosphorylation.**

200 IWS1 is phosphorylated by AKT3, and to a lesser extent by AKT1, at Ser720/Thr721
201 (Sanidas et al., 2014[14]). The preceding data show that IWS1 phosphorylation is required for
202 the nucleocytoplasmic export of RNAs transcribed from a set of intronless genes. This raised
203 the question of whether AKT, which phosphorylates IWS1 on Ser720/Thr721, is required for
204 the activation of the pathway. To address that, we treated NCI-H522 and NCI-H1299 cells with
205 5 μM of the pan-AKT inhibitor MK2206, a dose that fully inhibits all AKT isoforms (Sanidas et
206 al., 2014[14], Laliotis et al., 2020[15]). The results confirmed that MK2206 inhibits AKT (S473) and
207 IWS1 phosphorylation (S720) along with the *U2AF2* exon 2 inclusion, as expected (**Fig. 2A**).
208 Following proper fractionation of these cells upon treatment with MK2206 (**Fig. S2A**), we
209 examined the C/N ratio of *IFNA1, IFNB1* (induced by SeV-GFP infection), *JUN* and *HSBP3*
210 RNA with qPCR and their protein expression. The results confirmed that inhibition of AKT
211 kinase phenocopies the loss of phosphorylated IWS1 resulting in nuclear retention of
212 intronless RNAs and subsequent downregulation of their protein products in both NCI-H522
213 and NCI-H1299 cell lines (**Fig. 2B, 2C**). To determine whether it is the AKT3 isoform, which is
214 responsible for the observed effects of AKT inhibition, we transducted NCI-H522 and NCI-
215 H1299 cells with lentiviral shAKT3 construct, along with shControl (**Fig. 2D**) and we examined
216 its effects on the nucleocytoplasmic export and expression of the same set of RNAs, following

217 successful compartment fractionation (**Fig. S2B**). The results phenocopied the inhibition with
218 MK2206 (**Fig. 2E, 2F)**, providing evidence that the observed regulation of nucleocytoplasmic
219 export depends on the phosphorylation of IWS1 by AKT3, through *U2AF2* RNA splicing.

220 **IWS1 phosphorylation is required for the proper function of the Cytoplasmic**
221 **Accumulation Region Elements (CAR-E).**

222 It has been previously reported that the consensus of Cytoplasmic Accumulation
223 Region Element (CAR-E) functions by promoting the cytoplasmic accumulation of mRNAs and
224 the production of proteins (Lei et al., 2013[13]). To further study the role of IWS1 phosphorylation
225 in the function of the CAR-E, we used a previously described construct, in which 16 tandem
226 copies of the most conserved CAR-E (CCAGTTCCTG element of *JUN*) or its mutated version
227 (CAR-E_{mut}), were inserted upstream of β-globin cDNA (**Fig. 3A**) (Lei et al., 2013[13]). As controls,
228 pCMV promoter-driven constructs encoding β-globin cDNA alone or β-globin gene containing
229 its two natural introns were analyzed in parallel. Based on previous work, the β-globin gene
230 mRNA, efficiently accumulates in the cytoplasm, whereas the β-globin cDNA transcript, is
231 normally degraded in the nucleus (Dias et al., 2010[23], Lei et al., 2011[24], Valencia et al., 2008[25]).
232 Transient transfection of these constructs in shControl, shIWS1, shIWS1/WT-R,
233 shIWS1/MT-R, shIWS1/U2AF65α, and shIWS1/U2AF65β NCI-H522 and NCI-H1299 cells
234 (**Fig. 3B, S3A**), showed proper expression of the HA-β-globin gene in all conditions,
235 independent of IWS1 phosphorylation. Furthermore, consistent with previous reports, β-globin
236 cDNAs containing the inserted mutated CAR-E element (CAR-E_{mut}), employed a similar
237 nucleocytoplasmic accumulation to the β-globin cDNA transcripts alone, with limited protein
238 expression of β-globin detected in all conditions, due to nuclear retention. In addition, the
239 insertion of 16 tandem CAR-E was efficient to induce the expression of HA-β-globin in
240 shControl cells. Strikingly, the same construct was unable to promote the expression of CAR-
241 E HA-β-globin in shIWS1 and shIWS1/MT-R cells, a phenotype rescued in shIWS1/WT-R
242 cells. More importantly, the observed shIWS1 CAR-E HA-β-globin nuclear retention

243 phenotype was rescued by U2AF65α, but not U2AF65β. These results suggest that IWS1
244 phosphorylation is required for the maintenance of CAR-E function, through *U2AF2* RNA
245 splicing.

246 **The splicing of the *U2AF2* mRNA downstream of IWS1 phosphorylation regulates the**
247 **Prp19 recruitment on the CAR-E.**

248 Based on our previous data, IWS1 phosphorylation is required for the function of the
249 CAR-E (**Fig. 3**). As mentioned above, it has been previously demonstrated that U2AF65 and
250 Prp19 affect the nucleocytoplasmic export of naturally intronless RNAs, by binding to the CAR-
251 E (Lei et al., 2013[13]). Given that aberrant splicing of *U2AF2* in shIWS1 and shIWS1/MT-R cells
252 resulted in the loss of the interaction between U2AF65 and Prp19 (Laliotis et al., 2020[15]), we
253 hypothesized that IWS1 phosphorylation affects the recruitment of the regulatory U2AF65-
254 Prp19 complex to the CAR-E elements and, eventually, their function.

255 To address this hypothesis, we performed RNA Immunoprecipitation (RIP) assays in
256 shControl, shIWS1, shIWS1/WT-R, shIWS1/MT-R, shIWS1/U2AF65α and shIWS1/U2AF65β
257 NCI-H522 and NCI-H1299 cells, using a set of primers specifically amplifying the CAR-E or
258 control regions on *IFNA1, IFNB1, JUN and HSPB3* mRNAs (**Fig. S4A**). The results confirmed
259 that both spliced variants of U2AF65 bind equally well with the CAR-E, but not the control
260 sequences (**Fig. 4A, 4B upper panels**). However, Prp19 binding to the same CAR-E regions
261 was significantly impaired in shIWS1 and shIWS1/MT-R cells, which predominantly express
262 the U2AF65β isoform (**Fig. 4A lower panels**). More importantly, the impaired Prp19 binding
263 on the CAR-E was rescued by U2AF65α, but not U2AF65β (**Fig. 4B lower panels**). These
264 results suggest that IWS1 phosphorylation controls the nucleocytoplasmic export of RNAs
265 transcribed from intronless genes, by the regulation of the U2AF65-Prp19 interaction, through
266 *U2AF2* alternative RNA splicing.

267 To further investigate the activity of this pathway in Lung Adenocarcinoma patients
268 (LUAD), we used 3 high and 3 low p-IWS1 LUAD patients, as identified in our previous work

269 (Laliotis et al., 2020[15]). Western blot and RT-PCR analysis of these samples confirmed the
270 increased expression and phosphorylation of IWS1 in the high-expressing groups with parallel
271 inclusion of *U2AF2* exon 2 (**Fig. 4C upper panels**). Following successful fractionation (**Fig.**
272 **S4B**), qRT-PCR showed decreased Cytosolic/Nuclear ratio in the low p-IWS1 group, due to
273 nuclear retention of intronless mRNAs (**Fig. 4C lower panel**). More importantly, consistently
274 with the *in vitro* data, RIP experiments in the same tumor samples revealed increased binding
275 of U2AF65 on the CAR-E in both patient groups, independent of its splicing pattern, with
276 decreased recruitment of Prp19 on the CAR-E mRNA areas in the low p-IWS1 group, which
277 predominantly express the U2AF65β (**Fig. 4D**). These data suggest that the epigenetic
278 complexes that are controlled by IWS1 phosphorylation and regulate the RNA export of
279 intronless genes, are active in Lung Adenocarcinoma patients.

280 **RNA-Pol II affects the splicing-independent nuclear export of intronless genes.**

281 Based on previous reports, U2AF65 binds RNA Pol II, leading to an U2AF65-
282 dependent recruitment of Prp19 to the newly-synthesized pre-mRNA and promoting proper
283 co-transcriptional splicing activation (C.J David et. al., 2011[26]). In order to address the possible
284 involvement of RNA Pol II in the splicing-independent RNA export, we cloned *IFNA1* and
285 *IFNB1* cDNAs in the lentiviral vectors pLx304 and pLKO.1, which drive their expression
286 through CMV (RNA Pol II-dependent) and U6 (RNA Pol III-dependent) promoters, respectively
287 (**Fig. S5A**) (Schramm et al., 2002[27]). We then transduced NCI-H522 and NCI-H1299 cells with
288 lentiviral shIFNα1 or shIFNβ1, in order to remove the endogenous mRNA products.
289 Subsequently, we rescued their expression with the RNA Pol II (pLx304-R) or RNA Pol III-
290 driven (pLKO.1-R) lentiviral construct and addressed the expression of *IFNA1* or *IFNB1* with
291 qRT-PCR, following SeV-GFP infection. The results confirmed the significant downregulation
292 of *IFNA1* and *IFNB1* expression in the shIFNα and shIFNβ cells, respectively, with robust
293 expression in both pLx304-R and pLKO.1-R cells. (**Fig. 5A left panel**). To further investigate
294 the role of RNA Pol II in the nucleocytoplasmic export of type I IFNs, we fractionated the same
295 NCI-H522 and NCI-H1299 cells (**Fig. S5B**) and measured the C/N ratio with qRT-PCR,

296 following SeV-GFP infection. Interestingly, the results showed nuclear retention and
297 downregulation of IFNβ1 levels in the pLKO.1-R cells, an effect rescued in pLx304-R cells.
298 (**Fig. 5A right panels, 5B**). These results suggest that RNA Pol II is involved in the regulation
299 of the splicing-independent RNA export of naturally intronless RNAs.

300 **The loss of IWS1 phosphorylation enhances viral infection through the aberrant p-**
301 **STAT1 signaling and transcription of ISGs.**

302 The preceding data suggest that IWS1 phosphorylation affects the nucleocytoplasmic
303 export and expression of type I IFNs, through the regulation of the U2AF65-Prp19 interaction
304 and their recruitment to CAR-E elements of *IFNA1 and IFNB1* mRNAs. Given that type I IFNs
305 orchestrate the cellular antiviral response (Lazear et al., 2019[28]), we hypothesized that loss of
306 IWS1 phosphorylation will accordingly increase viral replication, due to the downregulation of
307 type I IFNs. To this extent, we infected NCI-H522 and NCI-H1299 shCon, shIWS1,
308 shIWS1/WT-R and shIWS1/MT-R cells with a set of viral strains including Vesicular Stomatitis
309 Virus (VSV-GFP), Sendai (SeV-GFP), Reovirus and Influenza A virus (IAV-GFP) and we
310 monitored the levels of infections with flow cytometry (Chesarino et al., 2015[29], Kenney et al.,
311 2019[30], Sermersheim et al., 2020[31]). To carry out these experiments we used short hairpin
312 RNA constructs in a pGIPZ vector we modified by deleting the GFP cassette. Consistently,
313 the results showed increased infection by all viral strains in shIWS1 and shIWS1/MT-R cells,
314 a phenotype rescued in shIWS1/WT-R cells, which parallels the nucleocytoplasmic distribution
315 and reduced expression of type I IFNs. (**Fig. 6A, S6A**).

316 Based on the latter data, we then questioned whether the observed downregulation of
317 type I IFNs upon the loss of phosphorylated IWS1 affects the IFN downstream signaling
318 pathways and the induction of Interferon Stimulated Genes (ISGs). To address this question,
319 we infected NCI-H522 shControl and shIWS1 cells with VSV-GFP virus. After 16h of infection,
320 the cells were harvested for RNA and the supernatant derived from each condition was used
321 to stimulate NCI-H522 parental cells, for various time intervals (**Fig. 5B**). Western blot analysis
322 of protein extracts from these intervals, revealed robust activation of p-STAT1 (Y701) after the

323 stimulation of NCI-H522 cells with shControl-derived supernatant, with a parallel expression
324 of IFNβ1, phenomenon not triggered by the stimulation with the shIWS1-derived supernatant
325 (**Fig. 5C, upper panel**).

326 The increase in the abundance of IFNβ1, within 10 minutes from the start of the
327 stimulation, was surprising because it was too rapid to be due by the induction of the *IFNB1*
328 gene. Previous studies had shown that IFNβ1 undergoes endocytosis and that it can be siloed
329 in endosomes, where it can be detected for days following IFN treatment (Altman et al.,
330 2020[32]). Based on this information, we hypothesized that IFNβ1 detected in this experiment
331 was endocytosed from the supernatants of shControl cells. To address this hypothesis we
332 treated parental NCI-H522 cells with recombinant human IFNβ1 and we probed the cell lysates
333 harvested at sequential time points with antibodies to IFNβ1. The results confirmed the rapid
334 accumulation of the recombinant IFNβ1 in the harvested cell lysates (**Fig. S6B**).

335 To further support our data, and given that p-STAT1 is a main component of the
336 Interferon Stimulated Gene Factor 3 (ISGF3) for the transcriptional induction of ISGs (Wang
337 et al., 2017[33]), we performed Chromatin Immuno Cleavage (ChIC) assays in NCI-H522 cells
338 stimulated for 30' with shControl or shIWS1-derived supernatant, along with unstimulated
339 cells. Consistent with the p-STAT1 activation pattern, the results showed increased binding of
340 p-STAT1 (Y701) to the Interferon Stimulated Response Elements (ISREs) of the major ISGs
341 *IRF1, IRF9, STAT1,* and *STAT2*, in the shControl-derived stimulated cells (**Fig. 6C, lower**
342 **panel**). Notably, total RNA extracted from NCI-H522 shControl, shIWS1, shIWS1/WT-R, and
343 shIWS1/MT-R cells following VSV-GFP infection, revealed robust downregulation of a set of
344 20 ISGs in shIWS1 and shIWS1/MT-R cells, a phenotype rescued in shIWS1/WT-R cells (**Fig.**
345 **6D**). More importantly, the treatment of NCI-H522 cells with the clinically used pan-AKT
346 inhibitor MK2206 followed by VSV-GFP infection phenocopied the ISGs signature
347 downregulation upon loss of IWS1 phosphorylation (**Fig. 6E**) and parallels the expression of
348 type IFNs and p-STAT1 activation. Altogether, these data suggest that IWS1 phosphorylation
349 by AKT kinase, regulates viral replication, through the nucleocytoplasmic export of type I IFNs
350 and the subsequent activation of p-STAT1 and induction of ISGs.

351 **Inhibition of the AKT/p-IWS1 axis sensitizes lung adenocarcinoma cells to oncolytic**
352 **viral killing.**

353 Based on the preceding data, loss of IWS1 phosphorylation enhances viral replication
354 by affecting the induction of p-STAT1 and ISGs, due to impaired type I IFNs expression. We
355 then hypothesized that IWS1 would affect the sensitivity of lung adenocarcinoma cells to
356 oncolytic viral infection, through the regulation of type I IFN response. To determine whether
357 IWS1 phosphorylation affects the sensitivity of lung adenocarcinoma cells to infection with
358 oncolytic viruses, we used the viral strains VSV-GFP and Reovirus, which are widely tested
359 as potential virotherapy in a variety of solid tumors, including lung cancer (Schreiber et al.,
360 2019[34], Villalona-Calero et al., 2016[35]). By infecting NCI-H522 and NCI-H1299 shControl,
361 shIWS1, shIWS1/WT-R, and shIWS1/MT-R cells with increasing Multiplicity of Infection (MOI),
362 we observed increased viral-induced killing of shIWS1 and shIWS1/MT-R cells by VSV and
363 Reovirus, after 16h and 48h of infection respectively, compared to shControl and shIWS1/WT-
364 R cells (**Fig. 7A, S7A**). It is worth mentioning that according to our previous observations, the
365 NCI-H522 and NCI-H1299 shIWS1 cells do not exhibit proliferation deficits upon 48h,
366 compared to the shControl cells, suggesting that the observed effect is solely due to the viral
367 infection (Laliotis et al., 2020[15]). More importantly, the treatment of NCI-H522 and NCI-H1299
368 cells with the pan-AKT inhibitor MK2206, sensitized the cancer cells to viral killing by VSV and
369 Reovirus, phenocopying the loss of IWS1 phosphorylation (**Fig. 7B, S7B**).

370 To further demonstrate the cellular events following the infection with the oncolytic
371 viruses, NCI-H522 and NCI-H1299 shControl and shIWS1 cells were infected with VSV
372 (MOI=1) for several time point intervals, and cleavage of PARP, a hallmark of Caspase-
373 mediated death, was examined by Western Blotting (Chaitanya et al., 2010[36]). Strikingly, the
374 results revealed robust PARP-cleavage in the shIWS1 cells, observed at the early time points
375 compared to the shControl cells, further supporting our hypothesis (**Fig. 7C, S7C**). These data
376 come in agreement with the effect of IWS1 phosphorylation on the nucleocytoplasmic

377 distribution of type I IFNs (**Fig. 1, Fig. 2**), the function of the CAR-E elements (**Fig. 3, Fig 4**),
378 the pattern of viral infection and the activation of p-STAT1 and the downstream ISGs (**Fig. 5**).
379 Altogether, these data confirm our model in which, IWS1 phosphorylation by AKT
380 kinase at S720/T721 controls the epigenetic regulation of *U2AF2* alternative RNA splicing,
381 leading to the inclusion of exon 2. The exon 2-containing U2AF65α isoform binds and recruits
382 Prp19 on the CAR-E of *IFNA1* and *IFNB1*, promoting their nucleocytoplasmic export. During
383 oncolytic viral infection, the latter facilitates proper type I IFN expression, activation of the p-
384 STAT1/ISGF3, and transcription of ISGs, enhancing the resistance of lung adenocarcinoma
385 cells to oncolytic viral infection (**Fig. 8**)

386 **Discussion**

387 Our results implicate IWS1 phosphorylation as a regulator of the nucleocytoplasmic
388 export of naturally intronless RNAs and the type I IFN response. We report a pathway initiated
389 by the AKT3-mediated phosphorylation of IWS1 (**Fig. 1, Fig. 2**), which induces the alternative
390 RNA splicing of *U2AF2* (Laliotis et al., 2020[37]). This shift in the alternative RNA splicing pattern
391 controls the interaction of U2AF65 with yet another splicing factor, Prp19. These two factors
392 interact and regulate the nucleocytoplasmic export and expression of naturally intronless
393 genes *IFNA1, IFNB1, JUN* and *HSPB3,* by affecting the function of CAR-E and directly binding
394 on these elements (**Fig. 3, Fig. 4**). Subsequently, our findings suggest that inhibition of this
395 pathway enhances viral replication in the infected cells, due to the downregulation of type I
396 IFNs. Notably, this effect on viral replication is mediated by aberrant activation of p-STAT1
397 signals and active transcription of ISGs (**Fig. 6**). Finally, this manipulation of type I IFNs
398 response through the inhibition of the AKT/p-IWS1 axis sensitizes lung adenocarcinoma cells
399 to oncolytic viral killing mediated by Caspase signals (**Fig. 7**).
400 An important conclusion, based on the data presented in this report, is that the
401 epigenetic regulation of alternative RNA splicing, through IWS1 phosphorylation, along with

402 the downstream effect on splicing machinery, affects the splicing-independent nuclear export
403 of naturally intronless mRNAs. AKT kinase-mediated signals, through IWS1 phosphorylation,
404 affect *U2AF2* alternative RNA splicing and the U2AF65-Prp19 interaction and their function on
405 the splicing-independent export. This is also supported by previous work showing that splicing
406 factors are also associated with CAR-E (Lei et al., 2013[13]) and that many of them interact with
407 adapter proteins of the export machinery (Müller-McNicoll et al., 2016[38]). These data provide
408 insight into the explanation that splicing factors provide the backbone for protein-protein
409 interactions with export machinery components, inducing the export of these genes. In
410 addition, we provide evidence that IWS1 phosphorylation is necessary for the function of the
411 CAR-E (**Fig. 3**). Given that these elements have been identified in the majority of intronless
412 genes (Lei et al., 2011[24], Valencia et al., 2008[25], Lei et al., 2013[13]), our data suggest a global
413 role of the AKT/p-IWS1 axis in the regulation of splicing-independent export, through *U2AF2*
414 RNA splicing.

415 Interestingly, although IWS1 phosphorylation affects the export of intronless genes,
416 our results also show a negative correlation of IWS1 with their RNA expression in cell lines
417 and LUAD patients (**Fig. 1**). Notably, the *U2AF2* RNA splicing pattern affects the expression
418 of type IFNs mRNA, but not the one of *JUN* and *HSBP3*. Based on our recent data, loss of
419 IWS1 phosphorylation promotes genomic instability, through a process dependent on *U2AF2*
420 RNA splicing, leading to cytosolic DNA and transcription upregulation of type IFNs (Laliotis et
421 al., 2020[39]). The exact role of this pathway in the transcriptional regulation of these genes will
422 be addressed in future studies.

423 Our data also indicate that RNA Pol II contributes to the regulation of the nuclear export
424 of intronless RNAs (**Fig. 5**). Nonetheless, components of the TREX complex have been shown
425 to be efficiently loaded onto mRNAs even in the absence of splicing and regulate this process
426 (Akef et al., 2015[40], Lee, E.S. et al., 2015[41], Lee, E.S. et al., 2020[42]). Given that the TREX
427 complex is recruited to target genes by RNA Pol II co-transcriptionally (Sträßer et al., 2002[43]),
428 this suggests that the observed effect of RNA Pol II in this process may be through the

429 recruitment of TREX complex on these intronless genes. The exact role of RNA Pol II in this
430 process will be elucidated in future studies.

431 In the present study, we also demonstrated that signals originating from AKT3 kinase
432 regulate viral replication due to the regulation of type I IFNs, through IWS1 phosphorylation.
433 Specifically, suppression of the AKT3/p-IWS1 axis disrupts the U2AF65-Prp19 interaction,
434 leading to nuclear retention and downregulation of type IFNs (**Fig. 1, Fig. 2**). The latter
435 enhances viral replication of a set of viral strains, due to impaired ISGs induction (**Fig. 6**). The
436 PI3K/Akt pathway appears to be associated with the host cell immune response to counteract
437 viral infection, in an isoform-specific manner (Diehl et al., 2013[44]). Based on our previous work,
438 AKT1 selectively phosphorylates EMSY and stimulates the expression of ISGs (Ezell et al.,
439 2012[11]). In the present work, we demonstrate the opposing role of the AKT3 isoform in the
440 expression of ISG, through IWS1 phosphorylation. The fact that the selective inhibition of
441 some of these pathways, such as the EMSY or the IWS1 pathway, had profound effects on
442 the sensitivity of the cells to viral infection, suggests that these pathways may not function
443 independently of each other and that their roles may not be additive, but synergistic. A recent
444 report, consistent with our findings, found that PI3K/AKT blockade enhances the replication of
445 Reovirus by repressing ISGs (Tian et al., 2015[45]). Importantly, our data also implicate that
446 alternative RNA splicing and RNA processing can regulate the immune and type I IFN
447 response during viral infection. Given the fact that aberrant splicing is known to contribute to
448 defects in IFN response and viral replication (Chauhan et al., 2019[46], Chang et al., 2017[47]),
449 our data support another layer of this regulation through RNA export and processing.

450 Our findings support that inhibition of the AKT/p-IWS1 axis sensitizes the cells to
451 oncolytic viral killing, through the manipulation of RNA processing and export. These results
452 come in agreement with previous reports supporting that PI3K/AKT inhibition sensitizes cancer
453 cells to oncolytic viral infection (Tong et al., 2015[48]). Interestingly, in the case of non-small cell
454 lung cancer (NSCLC), several reports have demonstrated the synergistic role of Reovirus and
455 VSV oncolytic viruses to the clinical outcome of lung cancer patients (Villalona-Calero et al.,
456 2016[35], Bishnoi et al., 2018[49]), with several ongoing clinical trials to date (NCT03029871,

457 NCT00861627). Notably, a preclinical *in vivo* lung cancer model with genetic ablation of
458 *IFNAR1* (*IFNAR1*$^{-/-}$*),* demonstrates synergistic therapeutic effects of VSV (Schreiber et al.,
459 2019[34]). Our data reveal that inhibition of the AKT/p-IWS1 axis downregulates the induction of
460 ISGs following VSV infection, including *IFNAR1* (**Fig. 6**), further supporting the role of the
461 AKT/IWS1 axis to the response to oncolytic viruses.

462 Another important clinical application of this pathway is that OVs often induce IFN
463 release in the Tumor Microenvironment (TME), resulting in an upregulation of PD-L1
464 expression on tumor cells (Bellucci et al., 2015[50]). Previous studies have shown that the
465 combination of Reovirus with PD-1 blockade enhanced the ability of NK cells to kill reovirus-
466 infected tumor cells, increased CD8+T cells, and enhanced the antitumor immune response
467 (Rajani et al., 2016[51]). Further studies proposed that a triple combination of anti–CTLA-4, anti–
468 PD-1, and oHSV–IL-12 resulted in long-term durable cures in most of the mice treated in two
469 syngeneic models of GBM by inducing a profound increase in the ratio of T effector to Tregs
470 (Saha et al., 2017[52]). More importantly, oncolytic viruses preferentially replicate in tumour cells
471 because the antiviral responses in these cells are dysfunctional (Xia et al., 2016[53]). In healthy
472 tissue, the production of interferons and interferon-related factors limits viral replication and
473 boosts the rate of viral clearance, suggesting limited potential side effects (Bommareddy et
474 al., 2018[54]). Driven by these strong evidences of the synergistic effect of OV with immune-
475 checkpoint inhibitors, several clinical trials have actively investigated the possible synergy
476 between these therapeutic approaches, with promising results (NCT02263508,
477 NCT02307149, NCT03153085).

478 The data in this report may also be relevant for the design of strategies to prevent or
479 overcome the resistance of *EGFR* mutant lung adenocarcinomas to Tyrosine kinase Inhibitors
480 (TKI). Our recent studies had shown that the IWS1 phosphorylation pathway is active in
481 human lung adenocarcinoma. More importantly, IWS1 phosphorylation and *U2AF2* exon 2
482 inclusion were shown to correlate positively with tumor stage, histologic grade and metastasis,
483 and to predict poor survival in patients with *EGFR* mutant, but not *KRAS* mutant tumors
484 (Laliotis et. al 2020[15]). A recent publication provided evidence, linking resistance to EGFR

485 inhibitors to the upregulation of type I IFN signaling (Gong et al., 2020[55]). This suggests that
486 by promoting type I IFN signaling, the IWS1 phosphorylation pathway may promote resistance
487 to EGFR TKI, contributing to the poor prognosis of these tumors.

488 Our data also show that the U2AF65/Prp19 spliceosomal complex that controls the
489 RNA export of intronless genes and recruited upon IWS1 phosphorylation, is active in Lung
490 Adenocarcinoma patients, suggesting it as a possible therapeutic target for the manipulation
491 of the IFN response in these patients. Based on the latter, we provide the rationale for three
492 potential translation applications. First, the combination of AKT/IWS1 inhibitors with oncolytic
493 viruses may enhance their lytic action in lung adenocarcinoma due to the suppression of the
494 induction of ISGs. Second, IWS1 inhibition could enhance the response of lung
495 adenocarcinoma patients treated with OV/PD-1 inhibitors, or the p-IWS1 levels may act as
496 precision medicine marker for response to OV or the OV/PD-1 blockade combination, through
497 the regulation of IFN response in the TME. Third, given that the IWS1 phosphorylation-
498 dependent effect on the response to oncolytic viruses is mediated through manipulation of
499 RNA splicing and RNA processing and a specific *U2AF2* isoform, a process occurring in LUAD
500 patients as well (**Fig. 4**), the oncolytic efficiency in lung adenocarcinoma patients may be
501 enhanced with the use of highly isoform-specific antisense oligonucleotides and
502 pharmacologic modulators of splicing machinery (Obeng et al., 2019[56]), which are currently
503 under clinical trials (NCT03901469, NCT02711956, NCT02268552, NCT02908685).

504 Collectively, our results describe a novel pathway through IWS1 phosphorylation by
505 AKT which, through the regulation of RNA processing and export machinery, may serve as a
506 precision-medicine marker for response and important synergy target for the therapeutic
507 outcome of oncolytic viral therapy in lung adenocarcinoma.

508

509 **Materials and Methods**

510 **Cells and culture conditions, transfections and inhibitors**

511 Cells, inhibitors and shRNAs, lentiviral constructs and experimental protocols are described in
512 detail in the supplemental experimental procedures. Experimental protocols include use of
513 inhibitors, transient transfections, lentiviral packaging, and cellular transduction with lentiviral
514 constructs.

515 **Expression Vectors and shRNAs**

516 The origin of the expression clones and shRNAs are described in Supplementary Table S3.
517 The cloning of *IFNA1* and *IFNB1* cDNA in the pLx304-V5 and pLKO.1 vectors is described in
518 the Supplementary Experimental Procedures. The pGIPZ shIWS1 clone used in this report
519 (Sanidas et al., 2014[14], Laliotis et al., 2020[15]), was subjected to modification in order to remove
520 the GFP cassette, are also described in the Supplementary Experimental Procedures.

521 **Immunoblotting**

522 Cells were lysed with RIPA buffer and cell lysates were resolved by electrophoresis in SDS-
523 PAGE and analyzed by immunoblotting. Images were acquired and analyzed, using the Li-
524 Cor Fc Odyssey Imaging System (LI-COR Biosciences, Lincoln, NE). For the lists of antibodies
525 used for immunoprecipitation and western blotting and for other details, see Supplemental
526 Experimental Procedures.

527 **Subcellular Fractionation**

528 Cell pellets were fractionated into nuclear and cytoplasmic fractions, which were used to
529 measure the relative abundance of proteins and RNAs in the nucleus and the cytoplasm, as
530 described before (Laliotis et al., 2020[15]). For details, see Supplemental Experimental
531 Procedures.

532 **RT-PCR and qRT-PCR**

533 Total RNA was isolated using the PureLink RNA Kit (Invitrogen, Cat. No 12183018A). Isolated
534 RNA was analyzed by real-time RT-PCR for the expression of the indicated mRNAs. The
535 mRNA levels were normalized based on the levels of GAPDH or 18S rRNA (internal control).
536 The primer sets used are listed in the Supplemental Experimental Procedures.

537 **Chromatin Immuno-Cleavage (ChIC)**

538 The binding of p-STAT1 on ISRE of ISGs was addressed by chromatin Immuno-cleavage
539 (Skene et al., 2018[57], Laliotis et al., 2020[15]). For details, for the ChIC protocols. see
540 Supplemental Experimental Procedures.

541 **Virus propagation and titering**

542 Influenza virus A/PR/8/1934 (H1N1) expressing green fluorescent protein (PR8-GFP) was
543 propagated in 10-day-old embryonated chicken eggs (Charles River Laboratories) for 48 hours
544 at 37°C and titered in MDCK cells. Sendai virus expressing GFP (SEV-GFP) was propagated
545 in 10-day-old embryonated chicken eggs at 37°C for 40 hours and titered on Vero cells. VSV
546 expressing GFP (VSV-GFP) was propagated and titered in HeLa cells. Reovirus was
547 propagated and titered in Vero cells.
548

549 **Cell infections and flow cytometry**

550 NCI-H522 cells were infected with PR8-GFP or Reovirus at an MOI of 1.0 for 24h, or with
551 VSV-GFP or SEV-GFP at an MOI of 0.5 for 16h. NCI-H1299 cells were infected with_PR8-
552 GFP at an MOI of 1.0 for 24h, or with VSV-GFP or SEV-GFP at an MOI of 0.25 for 24h.
553 Following infection, cells were fixed in 4% paraformaldehyde (Thermo Scientific),
554 permeabilized with 0.1% Triton X-100 in PBS, and incubated with PBS containing 2% fetal
555 bovine serum. Reovirus-infected cells were stained with anti-reovirus T3D sigma 3 antibody
556 (DSHB, 10G10), followed by anti-mouse Alexa488-conjugated secondary antibody (Thermo

557 Scientific, A-11029). PR8, VSV, and SEV infection rates were measured by detecting virus-
558 encoded GFP. Flow cytometry was performed on a FACSCanto II flow cytometer (BD
559 Biosciences) and analyzed using FlowJo software (DB, Ashland, OR).

560 **RNA Immunoprecipitation**

561 The binding of RNA binding proteins to regions of the IFNα, IFNβ, c-Jun and HSPB3 mRNAs
562 was addressed by RNA Immunoprecipitation, as described before (Laliotis et al., 2020[15]). For
563 details, see Supplemental Experimental Procedures.

564 **Cellular Survival/Killing curves**

565 For the determination of cell survival following oncolytic viral infections, NCI-H522 and NC-
566 H1299 cells were plated in 24-well plates. The cells were exposed to increased MOI of VSV
567 and Reovirus for 16h and 48h, respectively. After the incubation period, cell proliferation was
568 quantified by fluorescent detection of the reduction of resazurin to resorufin by viable cells and
569 normalized to DMSO-treated wells, using alamarBlue™ HS Cell Viability Reagent (Thermo
570 Fisher Cat. No A50100), as described in the Supplemental Experimental Procedures.

571 **TCGA/RPPA analysis**

572 TCGA data were downloaded from https://portal.gdc.cancer.gov/ and analysed as described
573 in the Supplemental Experimental Procedures.

574 **Data availability**

575 All the source data derived from this report have been deposited in the Mendeley Dataset.
576 (Laliotis et al., 2020[58], doi: 10.17632/853gfbbx7m.1)

577 **Statistical analysis**

578 All the statistical analysis was performed in GraphPad Prism, as described in the
579 corresponding section. All the statistical analysis reports can be found in the Mendeley dataset

580 where the source data of this report were deposited. (Laliotis et al., 2020[58], doi:
581 10.17632/853gfbbx7m.1)

582 **Acknowledgments**

583 The authors wish to thank all the members of the Tsichlis Lab for helpful discussions. We also
584 thank Dr Samir Achaya for reviewing the manuscript before the submission. This work was
585 supported by the NIH grant R01 CA186729 to P.N.T., the NIH grant R01 CA198117 to P.N.T
586 and V.C, by start-up funds from the OSUCCC to P.N.T,, from the National Center for
587 Advancing Translational Sciences grant KL2TR002734 to L.S. G.I.L is supported by the
588 Pelotonia Post-Doctoral fellowship from OSUCCC.

589 **Author Contributions**

590 **G.I.L.** Conceptualization, overall experimental design. Performed all the experiments except
591 the viral infections in Figure 6, analyzed the data, prepared the figures and wrote the
592 manuscript. **A.D.K.** Designed and performed all the infections with viral strains, optimized,
593 performed and analyzed the flow cytometry experiments and edited the manuscript **E.C.**
594 Designed and performed with G.I.L the time point interval experiment for p-STAT1 activation
595 and Caspase-mediated death in Figure 6 and Figure 7, edited the manuscript **A.O.** Assisted
596 to the time point interval experiment for Caspase-mediated death and edited the manuscript
597 **A.K.K** Performed the cloning of the type I IFN vectors for RNA Pol II and III promoter
598 expression, performed RT-PCR experiments **A.L.F.** Bioinformatics analyses of RNA-Seq and
599 TCGA data, edited the manuscript. **V.A.** Assisted to the time point interval experiment for p-
600 STAT1 activation and edited the manuscript **J.D.B** Advised on the design of experiments and
601 edited the manuscript **C.T.** Advised on the design of experiments and edited the manuscript.
602 **L.S.** Advised on the design of experiments and edited the manuscript **V.C.** Contributed to
603 overall experimental design, edited the manuscript. **J.S.Y** Designed the viral infection
604 experiments and contributed to overall experimental design, edited the manuscript **P.N.T.**
605 Overall experimental design, manuscript writing and editing.

606

607 **References**

608

609 1. Frisch, S.M. and MacFawn, I.P., 2020. Type I interferons and related pathways in cell
610 senescence. *Aging Cell*, p.e13234.
611 2. Acosta, P.L., Byrne, A.B., Hijano, D.R. and Talarico, L.B., 2020. Human Type I
612 Interferon Antiviral Effects in Respiratory and Re Emerging Viral Infections. *Journal of*
613 *Immunology Research*, *2020*.
614 3. Amarante-Mendes, G.P., Adjemian, S., Branco, L.M., Zanetti, L.C., Weinlich, R. and
615 Bortoluci, K.R., 2018. Pattern recognition receptors and the host cell death molecular
616 machinery. *Frontiers in immunology*, *9*, p.2379.
617 4. Ablasser, A. and Hur, S., 2019. Regulation of cGAS-and RLR-mediated immunity to
618 nucleic acids. *Nature Immunology*, pp.1-13.
619 5. Aleynick, M., Svensson-Arvelund, J., Flowers, C.R., Marabelle, A. and Brody, J.D.,
620 2019. Pathogen molecular pattern receptor agonists: treating cancer by mimicking
621 infection. *Clinical Cancer Research*, *25*(21), pp.6283-6294.
622 6. Park, A.K., Fong, Y., Kim, S.I., Yang, J., Murad, J.P., Lu, J., Jeang, B., Chang, W.C.,
623 Chen, N.G., Thomas, S.H. and Forman, S.J., 2020. Effective combination
624 immunotherapy using oncolytic viruses to deliver CAR targets to solid tumors. *Science*
625 *Translational Medicine*, *12*(559).
626 7. Rehman, H., Silk, A.W., Kane, M.P. and Kaufman, H.L., 2016. Into the clinic:
627 Talimogene laherparepvec (T-VEC), a first-in-class intratumoral oncolytic viral therapy.
628 *Journal for immunotherapy of cancer*, *4*(1), pp.1-8.
629 8. Martinez-Quintanilla, J., Seah, I., Chua, M. and Shah, K., 2019. Oncolytic viruses:
630 overcoming translational challenges. *The Journal of Clinical Investigation*, *129*(4),
631 pp.1407-1418.

632 9. Kroczynska, B., Mehrotra, S., Arslan, A.D., Kaur, S. and Platanias, L.C., 2014.
633 Regulation of interferon-dependent mRNA translation of target genes. *Journal of*
634 *Interferon & Cytokine Research*, *34*(4), pp.289-296.
635 10. Gantner, B.N., Jin, H., Qian, F., Hay, N., He, B. and Richard, D.Y., 2012. The Akt1
636 isoform is required for optimal IFN-β transcription through direct phosphorylation of β-
637 catenin. *The Journal of Immunology*, *189*(6), pp.3104-3111.
638 11. Ezell, S.A., Polytarchou, C., Hatziapostolou, M., Guo, A., Sanidas, I., Bihani, T., Comb,
639 M.J., Sourvinos, G. and Tsichlis, P.N., 2012. The protein kinase Akt1 regulates the
640 interferon response through phosphorylation of the transcriptional repressor EMSY.
641 *Proceedings of the National Academy of Sciences*, *109*(10), pp.E613-E621.
642 12. de Padilla, C.M.L. and Niewold, T.B., 2016. The type I interferons: Basic concepts and
643 clinical relevance in immune-mediated inflammatory diseases. *Gene*, *576*(1), pp.14-
644 21.
645 13. Lei, H., Zhai, B., Yin, S., Gygi, S. and Reed, R., 2013. Evidence that a consensus
646 element found in naturally intronless mRNAs promotes mRNA export. *Nucleic acids*
647 *research*, *41*(4), pp.2517-2525.
648 14. Sanidas, I., Polytarchou, C., Hatziapostolou, M., Ezell, S.A., Kottakis, F., Hu, L., Guo,
649 A., Xie, J., Comb, M.J., Iliopoulos, D. and Tsichlis, P.N., 2014. Phosphoproteomics
650 screen reveals akt isoform-specific signals linking RNA processing to lung cancer.
651 *Molecular cell*, *53*(4), pp.577-590.
652 15. Georgios I. Laliotis, Evangelia Chavdoula, Maria D. Paraskevopoulou, Abdul D. Kaba,
653 Alessandro La Ferlita, Satishkumar Singh, Vollter Anastas, Salvatore Alaimo, Arturo
654 Orlacchio, Keith A. Nair II, Vasiliki Taraslia, Ioannis Vlachos, Marina Capece,
655 ArtemisHatzigeorgiou, Dario I. Palmieri, Christos Tsatsanis, Lalit Sehgal, David P.
656 Carbone, Vincenzo Coppola, Philip N. Tsichlis, 2020 'IWS1 phosphorylation promotes
657 cell proliferation and predicts poor prognosis in EGFR mutant lung adenocarcinoma
658 patients, through the cell cycle-regulated U2AF2 RNA
659 splicing.bioRxiv2020.07.14.195297; doi: https://doi.org/10.1101/2020.07.14.195297

660 16. Georgios I. Laliotis, Evangelia Chavdoula, Maria D. Paraskevopoulou, Vollter Anastas,
661 Ioannis Vlachos, Vasiliki Tarasslia, Artemis Hatzigeorgiou, Dario Palmieri, Abdul Kaba,
662 Marina Capece, Arturo Orlacchio, Lalit Sehgal, Vincenzo Coppola and Philip N.
663 Tsichlis, Alternative RNA splicing of U2AF2, induced by AKT3-phosphorylated IWS1,
664 promotes tumor growth, by activating a CDCA5-pERK positive feedback loop, Cancer
665 Res August 15 2020 (80) (16 Supplement) 3649; **DOI:**10.1158/1538-7445.AM2020-
666 3649
667 17. Hogg, R., McGrail, J.C. and O'Keefe, R.T., 2010. The function of the NineTeen
668 Complex (NTC) in regulating spliceosome conformations and fidelity during pre-mRNA
669 splicing.
670 18. Chanarat, S. and Sträßer, K., 2013. Splicing and beyond: the many faces of the Prp19
671 complex. *Biochimica et Biophysica Acta (BBA)-Molecular Cell Research*, *1833*(10),
672 pp.2126-2134.
673 19. Yount, J.S., Kraus, T.A., Horvath, C.M., Moran, T.M. and López, C.B., 2006. A novel
674 role for viral-defective interfering particles in enhancing dendritic cell maturation. *The*
675 *Journal of Immunology*, *177*(7), pp.4503-4513.
676 20. Bedsaul, J.R., Zaritsky, L.A. and Zoon, K.C., 2016. Type I interferon-mediated
677 induction of antiviral genes and proteins fails to protect cells from the cytopathic effects
678 of Sendai virus infection. *Journal of Interferon & Cytokine Research*, *36*(11), pp.652-
679 665.
680 21. Szklarczyk, D., Gable, A.L., Lyon, D., Junge, A., Wyder, S., Huerta-Cepas, J.,
681 Simonovic, M., Doncheva, N.T., Morris, J.H., Bork, P. and Jensen, L.J., 2019. STRING
682 v11: protein–protein association networks with increased coverage, supporting
683 functional discovery in genome-wide experimental datasets. *Nucleic acids research*,
684 *47*(D1), pp.D607-D613.
685 22. Subramanian, A., Tamayo, P., Mootha, V.K., Mukherjee, S., Ebert, B.L., Gillette, M.A.,
686 Paulovich, A., Pomeroy, S.L., Golub, T.R., Lander, E.S. and Mesirov, J.P., 2005. Gene
687 set enrichment analysis: a knowledge-based approach for interpreting genome-wide

688 expression profiles. *Proceedings of the National Academy of Sciences*, *102*(43),
689 pp.15545-15550.
690 23. Dias, A.P., Dufu, K., Lei, H. and Reed, R., 2010. A role for TREX components in the
691 release of spliced mRNA from nuclear speckle domains. *Nature communications*, *1*(1),
692 pp.1-10.
693 24. Lei, H., Dias, A.P. and Reed, R., 2011. Export and stability of naturally intronless
694 mRNAs require specific coding region sequences and the TREX mRNA export
695 complex. *Proceedings of the National Academy of Sciences*, *108*(44), pp.17985-
696 17990.
697 25. Valencia, P., Dias, A.P. and Reed, R., 2008. Splicing promotes rapid and efficient
698 mRNA export in mammalian cells. *Proceedings of the National Academy of Sciences*,
699 *105*(9), pp.3386-3391.
700 26. David, C.J., Boyne, A.R., Millhouse, S.R. and Manley, J.L., 2011. The RNA polymerase
701 II C-terminal domain promotes splicing activation through recruitment of a U2AF65–
702 Prp19 complex. *Genes & development*, *25*(9), pp.972-983.
703 27. Schramm, L. and Hernandez, N., 2002. Recruitment of RNA polymerase III to its target
704 promoters. *Genes & development*, *16*(20), pp.2593-2620.
705 28. Lazear, H.M., Schoggins, J.W. and Diamond, M.S., 2019. Shared and distinct functions
706 of type I and type III interferons. *Immunity*, *50*(4), pp.907-923.
707 29. Chesarino, N.M., McMichael, T.M. and Yount, J.S., 2015. E3 ubiquitin ligase NEDD4
708 promotes influenza virus infection by decreasing levels of the antiviral protein IFITM3.
709 *PLoS Pathog*, *11*(8), p.e1005095.
710 30. Kenney, A.D., McMichael, T.M., Imas, A., Chesarino, N.M., Zhang, L., Dorn, L.E., Wu,
711 Q., Alfaour, O., Amari, F., Chen, M. and Zani, A., 2019. IFITM3 protects the heart
712 during influenza virus infection. *Proceedings of the National Academy of Sciences*,
713 *116*(37), pp.18607-18612.
714 31. Sermersheim, M., Kenney, A.D., Lin, P.H., McMichael, T.M., Cai, C., Gumpper, K.,
715 Adesanya, T.A., Li, H., Zhou, X., Park, K.H. and Yount, J.S., 2020. MG53 suppresses

716 interferon-β and inflammation via regulation of ryanodine receptor-mediated
717 intracellular calcium signaling. *Nature communications*, *11*(1), pp.1-12.
718 32. Altman, J.B., Taft, J., Wedeking, T., Gruber, C.N., Holtmannspötter, M., Piehler, J. and
719 Bogunovic, D., 2020. Type I IFN is siloed in endosomes. *Proceedings of the National*
720 *Academy of Sciences*, *117*(30), pp.17510-17512.
721 33. Wang, W., Xu, L., Su, J., Peppelenbosch, M.P. and Pan, Q., 2017. Transcriptional
722 regulation of antiviral interferon-stimulated genes. *Trends in microbiology*, *25*(7),
723 pp.573-584.
724 34. Schreiber, L.M., Urbiola, C., Das, K., Spiesschaert, B., Kimpel, J., Heinemann, F.,
725 Stierstorfer, B., Müller, P., Petersson, M., Erlmann, P. and von Laer, D., 2019. The lytic
726 activity of VSV-GP treatment dominates the therapeutic effects in a syngeneic model
727 of lung cancer. *British journal of cancer*, *121*(8), pp.647-658.
728 35. Villalona-Calero, M.A., Lam, E., Otterson, G.A., Zhao, W., Timmons, M.,
729 Subramaniam, D., Hade, E.M., Gill, G.M., Coffey, M., Selvaggi, G. and Bertino, E.,
730 2016. Oncolytic reovirus in combination with chemotherapy in metastatic or recurrent
731 non–small cell lung cancer patients with K RAS-activated tumors. *Cancer*, *122*(6),
732 pp.875-883.
733 36. Chaitanya, G.V., Alexander, J.S. and Babu, P.P., 2010. PARP-1 cleavage fragments:
734 signatures of cell-death proteases in neurodegeneration. *Cell Communication and*
735 *Signaling*, *8*(1), p.31.
736 37. Georgios I. Laliotis, Evangelia Chavdoula, Maria D. Paraskevopoulou, Vollter Anastas,
737 Ioannis Vlachos, Vasiliki Tarasslia, Artemis Hatzigeorgiou, Dario Palmieri, Abdul Kaba,
738 Marina Capece, Arturo Orlacchio, Lalit Sehgal, Vincenzo Coppola, Philip N. Tsichlis.
739 Alternative RNA splicing of U2AF2, induced by AKT3-phosphorylated IWS1, promotes
740 tumor growth, by activating a CDCA5-pERK positive feedback loop [abstract]. In:
741 Proceedings of the Annual Meeting of the American Association for Cancer Research
742 2020; 2020 Apr 27-28 and Jun 22-24. Philadelphia (PA): AACR; Cancer Res
743 2020;80(16 Suppl):Abstract nr 3649.

744 38. Müller-McNicoll, M., Botti, V., de Jesus Domingues, A.M., Brandl, H., Schwich, O.D.,
745 Steiner, M.C., Curk, T., Poser, I., Zarnack, K. and Neugebauer, K.M., 2016. SR
746 proteins are NXF1 adaptors that link alternative RNA processing to mRNA export.
747 *Genes & development*, *30*(5), pp.553-566.
748 39. Georgios I. Laliotis, Evangelia Chavdoula, Maria D. Paraskevopoulou, Abdul Kaba,
749 Alessandro La Ferlita, Vollter Anastas, Arturo Orlacchio, Vasiliki Taraslia, Ioannis
750 Vlachos, Marina Capece, Artemis Hatzigeorgiou, Dario Palmieri, Salvatore Alaimo,
751 Christos Tsatsanis, Lalit Sehgal, David P. Carbone, Vincenzo Coppola, Philip N.
752 Tsichlis. IWS1 phosphorylation promotes tumor growth and predicts poor prognosis in
753 EGFR mutant lung adenocarcinoma patients, through the epigenetic regulation of
754 U2AF2 RNA splicing [abstract]. In: Abstracts: AACR Special Virtual Conference on
755 Epigenetics and Metabolism; October 15-16, 2020; 2020 Oct 15-16. Philadelphia (PA):
756 AACR; Cancer Res 2020;80(23 Suppl):Abstract nr PO-011.
757 40. Akef, A., Lee, E.S. and Palazzo, A.F., 2015. Splicing promotes the nuclear export of
758 β-globin mRNA by overcoming nuclear retention elements. *RNA*, *21*(11), pp.1908-
759 1920.
760 41. Lee, E.S., Akef, A., Mahadevan, K. and Palazzo, A.F., 2015. The consensus 5'splice
761 site motif inhibits mRNA nuclear export. *PLoS One*, *10*(3), p.e0122743.
762 42. Eliza S Lee, Eric J Wolf, Sean S J Ihn, Harrison W Smith, Andrew Emili, Alexander F
763 Palazzo, TPR is required for the efficient nuclear export of mRNAs and lncRNAs from
764 short and intron-poor genes, *Nucleic Acids Research*, , gkaa919
765 43. Sträßer, K., Masuda, S., Mason, P., Pfannstiel, J., Oppizzi, M., Rodriguez-Navarro, S.,
766 Rondón, A.G., Aguilera, A., Struhl, K., Reed, R. and Hurt, E., 2002. TREX is a
767 conserved complex coupling transcription with messenger RNA export. *Nature*,
768 *417*(6886), pp.304-308.
769 44. Diehl, N. and Schaal, H., 2013. Make yourself at home: viral hijacking of the PI3K/Akt
770 signaling pathway. *Viruses*, *5*(12), pp.3192-3212.

771 45. Tian, J., Zhang, X., Wu, H., Liu, C., Li, Z., Hu, X., Su, S., Wang, L.F. and Qu, L., 2015.
772 Blocking the PI3K/AKT pathway enhances mammalian reovirus replication by
773 repressing IFN-stimulated genes. *Frontiers in microbiology*, *6*, p.886.
774 46. Chauhan, K., Kalam, H., Dutt, R. and Kumar, D., 2019. RNA Splicing: A New Paradigm
775 in Host–Pathogen Interactions. *Journal of molecular biology*, *431*(8), pp.1565-1575
776 47. Chang, M.X. and Zhang, J., 2017. Alternative Pre-mRNA splicing in mammals and
777 teleost fish: an effective strategy for the regulation of immune responses against
778 pathogen infection. *International journal of molecular sciences*, *18*(7), p.1530.
779 48. Tong, Y., Zhu, W., Huang, X., You, L., Han, X., Yang, C. and Qian, W., 2014. PI3K
780 inhibitor LY294002 inhibits activation of the Akt/mTOR pathway induced by an
781 oncolytic adenovirus expressing TRAIL and sensitizes multiple myeloma cells to the
782 oncolytic virus. *Oncology reports*, *31*(4), pp.1581-1588.
783 49. Bishnoi, S., Tiwari, R., Gupta, S., Byrareddy, S.N. and Nayak, D., 2018. Oncotargeting
784 by vesicular stomatitis virus (VSV): advances in cancer therapy. *Viruses*, *10*(2), p.90.
785 50. Bellucci, R., Martin, A., Bommarito, D., Wang, K., Hansen, S.H., Freeman, G.J. and
786 Ritz, J., 2015. Interferon-γ-induced activation of JAK1 and JAK2 suppresses tumor cell
787 susceptibility to NK cells through upregulation of PD-L1 expression. *Oncoimmunology*,
788 *4*(6), p.e1008824.
789 51. Rajani, K., Parrish, C., Kottke, T., Thompson, J., Zaidi, S., Ilett, L., Shim, K.G., Diaz,
790 R.M., Pandha, H., Harrington, K. and Coffey, M., 2016. Combination therapy with
791 reovirus and anti-PD-1 blockade controls tumor growth through innate and adaptive
792 immune responses. *Molecular Therapy*, *24*(1), pp.166-174.
793 52. Saha, D., Martuza, R.L. and Rabkin, S.D., 2017. Macrophage polarization contributes
794 to glioblastoma eradication by combination immunovirotherapy and immune
795 checkpoint blockade. *Cancer cell*, *32*(2), pp.253-267.
796 53. Xia, T., Konno, H., Ahn, J. and Barber, G.N., 2016. Deregulation of STING signaling in
797 colorectal carcinoma constrains DNA damage responses and correlates with
798 tumorigenesis. *Cell reports*, *14*(2), pp.282-297.

799 54. Bommareddy, P.K., Shettigar, M. and Kaufman, H.L., 2018. Integrating oncolytic
800 viruses in combination cancer immunotherapy. *Nature Reviews Immunology*, *18*(8),
801 p.498.
802 55. Gong, K., Guo, G., Panchani, N., Bender, M.E., Gerber, D.E., Minna, J.D., Fattah, F.,
803 Gao, B., Peyton, M., Kernstine, K. and Mukherjee, B., 2020. EGFR inhibition triggers
804 an adaptive response by co-opting antiviral signaling pathways in lung cancer. *Nature*
805 *Cancer*, *1*(4), pp.394-409.
806 56. Obeng, E.A., Stewart, C. and Abdel-Wahab, O., 2019. Altered RNA Processing in
807 Cancer Pathogenesis and Therapy. *Cancer discovery*, *9*(11), pp.1493-1510.
808 57. Skene, P.J. and Henikoff, S., 2017. An efficient targeted nuclease strategy for high-
809 resolution mapping of DNA binding sites. *Elife*, *6*, p.e21856.
810 58. Laliotis, Georgios I.; Kenney, Adam D.; Chavdoula, Evangelia; Orlacchio, Arturo;
811 Kaba, Abdul; La Ferlita, Alessandro; Anastas, Vollter; Beane, Joal D.; Tsatsanis,
812 Christos; Sehgal, Lalit; Coppola, Vincenzo D.; Yount, Jacob; Tsichlis, Philip N. (2020),
813 “IWS1 phosphorylation controls nucleocytoplasmic export of type I IFNs and the
814 sensitivity to oncolytic viruses, through U2AF2 RNA splicing”, Mendeley Data, V1, doi:
815 10.17632/853gfbbx7m.1

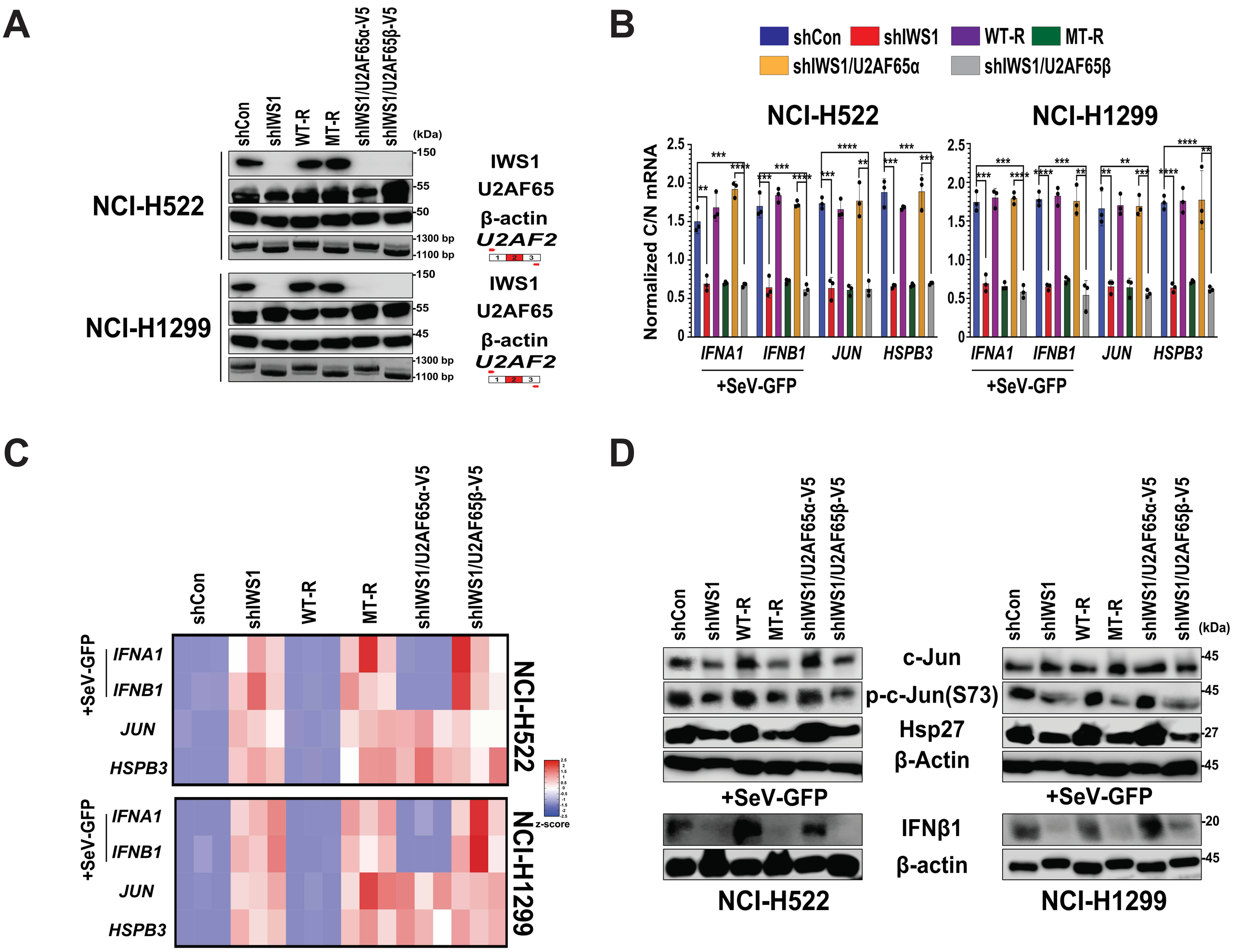
A
shCon
shIWS1
WT-R
MT-R
shIWS1/U2AF65α-V5
shIWS1/U2AF65β-V5
(kDa)
NCI-H522
NCI-H1299
IWS1
U2AF65
β-actin
U2AF2
150
55
50
45
1300 bp
1100 bp
B
shCon
shIWS1
WT-R
MT-R
shIWS1/U2AF65α
shIWS1/U2AF65β
NCI-H522
NCI-H1299
Normalized C/N mRNA
IFNA1
IFNB1
JUN
HSPB3
+SeV-GFP
C
z-score
D
c-Jun
p-c-Jun(S73)
Hsp27
β-Actin
IFNβ1
β-actin
+SeV-GFP
NCI-H522
NCI-H1299

Figure 1. IWS1 phosphorylation regulates the nucleocytoplasmic transport of mRNAs transcribed from a set of intronless genes, via *U2AF2* alternative RNA splicing.

A. Western blots of lysates of NCI-H522 and NCI-H1299 cells, transduced with the indicated constructs, were probed with anti-IWS1, anti-U2AF65 and anti-β-actin (control) antibodies. (first three lanes). RT-PCR of *U2AF2*, using oligonucleotide primers that map in exons 1 and 3 (fourth lane).

B. *IWS1 phosphorylation regulates the nucleocytoplasmic export of intronless mRNAs.* The same NCI-H522 (right panel) and NCI-H1299 (right panel) cells as in Fig. 1A, were fractionated into cytoplasmic and nuclear fractions. *IFNA1, IFNB1, JUN, HSPB3* and *GAPDH* mRNA levels in each fraction were determined using qRT–PCR. For each transcript, values are represented as cytoplasmic to nuclear ratios and were normalized to 18S rRNA. For type I IFN induction SeV-GFP infection was performed. The accuracy of the fractionation was validated with the experiment in Figure S1A. Bars show the mean normalized Cytosolic/Nuclear ratio ±SD

C. Total RNA was harvested from NCI-H522 (upper panel) and NCI-H1299 cells (lower panel), transduced with the indicated constructs. The expression of *IFNA1, IFNB1, JUN and HSPB3* mRNAs was determined by qRT-PCR and normalized to 18S rRNA. The results are represented as heatmap using z-scores from three individual biological experiments. For type I IFN induction SeV-GFP infection was performed. All assays in this figure were done in triplicate, on three biological replicates. n.s : non-significant *$p<0.05$, **$p<0.01$, ***$p<0.001$, ****$p<0.0001$. (one-side unpaired t-test).

D. Western blots of lysates of NCI-H522 (left panel) and NCI-H1299 (right panel) cells, transduced with the indicated constructs, were probed with anti-c-Jun, anti-p-c-Jun (S73), anti-Hsp27, anti-IFNβ1 and anti-β-actin (control) antibodies. For type I IFN induction SeV-GFP infection was performed. Throughout this figure NCI-H522 and NCI-H1299 cells were infected with MOI of 0.5 for 16h and MOI of 0.25 for 24h of SeV-GFP virus, respectively.

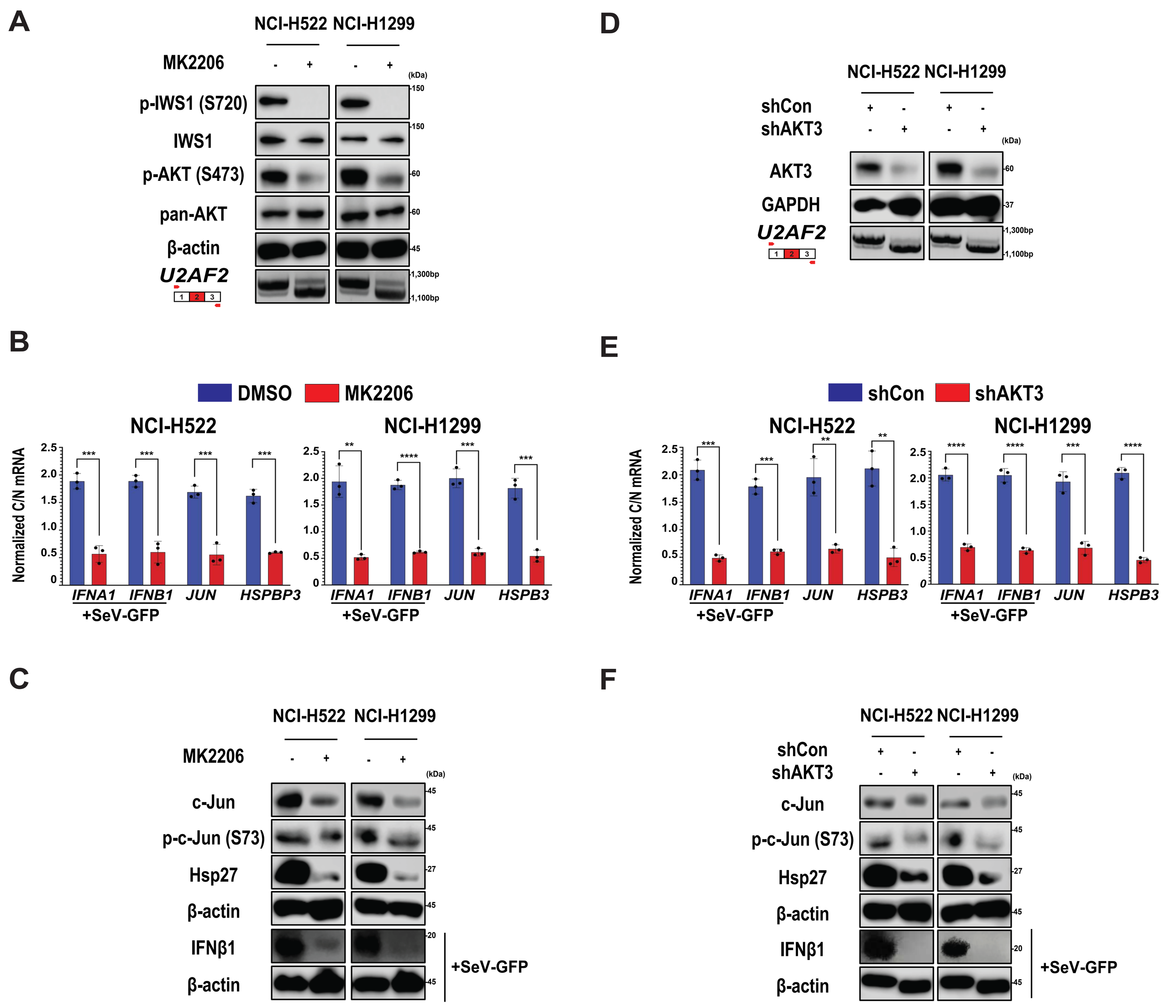
A
NCI-H522 NCI-H1299
MK2206
- + - +
(kDa)
p-IWS1 (S720)
IWS1
p-AKT (S473)
pan-AKT
β-actin
U2AF2
150
150
60
60
45
1,300bp
1,100bp
B
DMSO
MK2206
NCI-H522
NCI-H1299
Normalized C/N mRNA
IFNA1 IFNB1 JUN HSPBP3
IFNA1 IFNB1 JUN HSPB3
+SeV-GFP
C
NCI-H522 NCI-H1299
MK2206
- + - +
(kDa)
c-Jun
p-c-Jun (S73)
Hsp27
β-actin
IFNβ1
β-actin
45
45
27
45
20
45
+SeV-GFP
D
NCI-H522 NCI-H1299
shCon
shAKT3
+ - + -
- + - +
(kDa)
AKT3
GAPDH
U2AF2
60
37
1,300bp
1,100bp
E
shCon
shAKT3
NCI-H522
NCI-H1299
Normalized C/N mRNA
IFNA1 IFNB1 JUN HSPB3
IFNA1 IFNB1 JUN HSPB3
+SeV-GFP
F
NCI-H522 NCI-H1299
shCon
shAKT3
+ - + -
- + - +
(kDa)
c-Jun
p-c-Jun (S73)
Hsp27
β-actin
IFNβ1
β-actin
45
45
27
45
20
45
+SeV-GFP

Figure 2. AKT3 kinase affects the nucleocytoplasmic export of RNAs transcribed from intronless genes, thought IWS1 phosphorylation

A. NCI-H522 and NCI-H1299 cell lysates, harvested following a 4 hr treatment with MK2206 (5μM) or DMSO, were probed with the indicated antibodies. (Lower lane) RT-PCR reactions, using mRNA derived from the cells in the upper panel and oligonucleotide primers mapping in *U2AF2* exons 1 and 3 show that inhibiting Akt inhibits the inclusion of exon 2 in mature *U2AF2* mRNA transcripts in both cell lines.

B. *AKT kinase regulates the nucleocytoplasmic export of intronless mRNAs, through IWS1 phosphorylation.* Cells after similar treatment as Fig. 2A, were fractionated into cytoplasmic and nuclear fractions, *IFNα1, IFNβ1, c-Jun, HSPB3* and *GAPDH* mRNA levels in each fraction were determined using qRT–PCR. For each transcript, values are represented as cytoplasmic to nuclear ratios and were normalized to 18S rRNA. For type I IFN induction SeV-GFP infection was performed. The accuracy of the fractionation was validated with the experiment in Figure S2A. Bars show the mean normalized Cytosolic/Nuclear ratio ±SD

C. NCI-H522 and NCI-H1299 cell lysates as in Fig. 2A, were probed with the indicated antibodies. For type I IFN induction SeV-GFP infection was performed.

D. NCI-H522 and NCI-H1299 cells were transduced with lentiviral shAKT3 constructs along with shControl and their protein lysates were probed with the indicated antibodies

E. The indicated cells were fractionated into cytoplasmic and nuclear fractions, *IFNα1, IFNβ1, c-Jun, HSPB3* and *GAPDH* mRNA levels in each fraction were determined using qRT–PCR. For each transcript, values are represented as cytoplasmic to nuclear ratios and were normalized to 18S rRNA. For type I IFN induction SeV-GFP infection was performed. The accuracy of the fractionation was validated with the experiment in Figure S2B. Bars show the mean normalized Cytosolic/Nuclear ratio ±SD

F. NCI-H522 and NCI-H1299 cell lysates as in Fig. 2D, were probed with the indicated antibodies. For type IFN induction SeV-GFP infection was performed. Throughout this figure NCI-H522 and NCI-H1299 cells were infected with MOI of 0.5 for 16h and MOI of 0.25 for 24h of SeV-GFP virus, respectively. All assays in this figure were done in triplicate, on three biological replicates. n.s : non-significant *$p<0.05$, **$p<0.01$, ***$p<0.001$, ****$p<0.0001$. (one-side unpaired t-test).

A

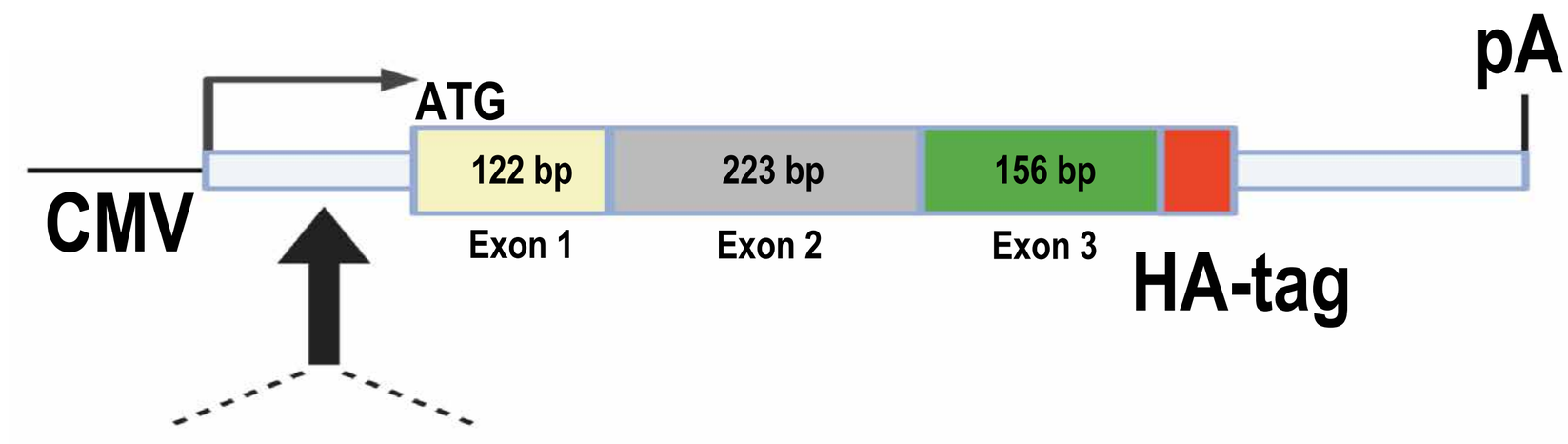

CAR-E (CCAGTTCCTG) x16

CAR-E mut (ggAGTTCCTG) x16

B

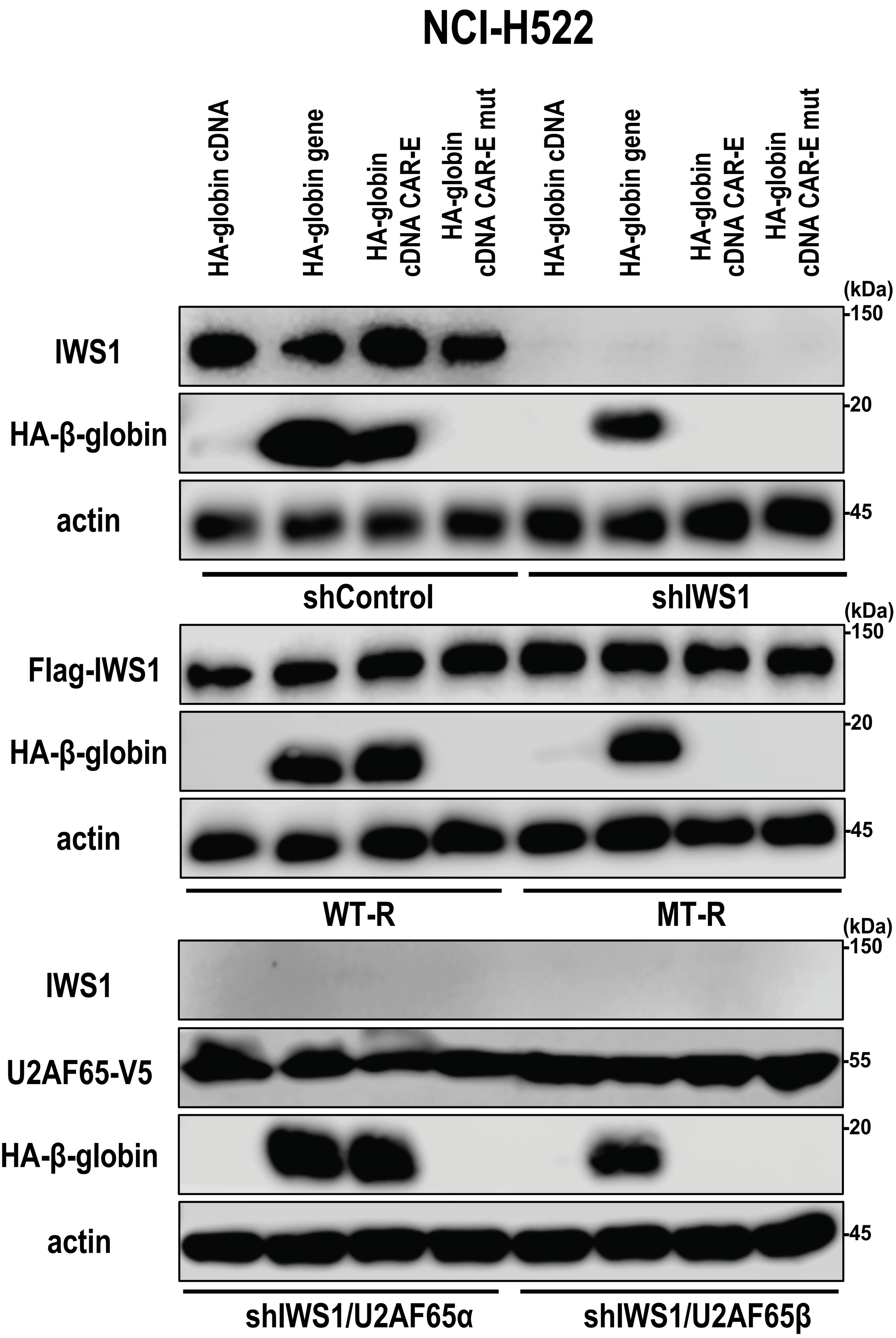

Figure 3. IWS1 phosphorylation is required for the proper function of the CAR-E elements.

A. Schematic representation of pCMV human β-globin cDNA construct indicating the position where the CAR-E and CAR-E_{mut} were inserted, as described before (Lei et al., 2013[13]). The start codon (ATG), HA tag and BGH polyA signal (pA) are indicated. The exon sizes (in bp) are shown.

B. *IWS1 phosphorylation is required for CAR-E function.* NCI-H522 cells transduced with the indicated constructs, were transfected transiently with pCMV HA-β-globin cDNA, HA-β-globin wt, HA-β-globin CAR-E and HA-β-globin CAR-E_{mut}. After 48h were harvested, and their lysates were probed with the indicated antibodies.

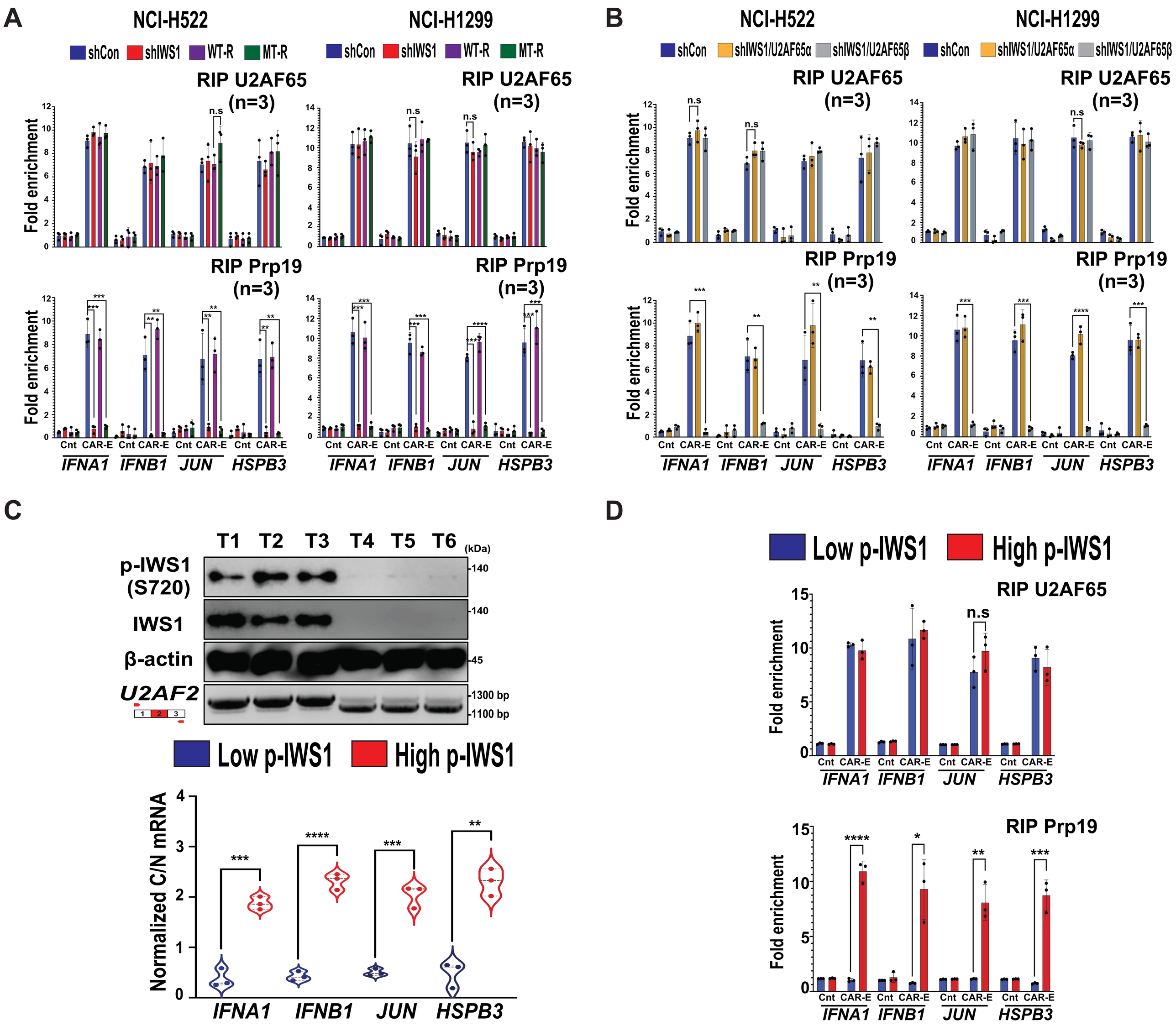
A
NCI-H522
NCI-H1299
shCon
shIWS1
WT-R
MT-R
RIP U2AF65 (n=3)
RIP Prp19 (n=3)
Fold enrichment
n.s
Cnt
CAR-E
IFNA1
IFNB1
JUN
HSPB3
B
shIWS1/U2AF65α
shIWS1/U2AF65β
C
T1
T2
T3
T4
T5
T6
(kDa)
p-IWS1 (S720)
IWS1
β-actin
U2AF2
140
45
1300 bp
1100 bp
Low p-IWS1
High p-IWS1
Normalized C/N mRNA
D

Figure 4. The splicing of the *U2AF2* mRNA downstream of IWS1 phosphorylation, regulates the Prp19 recruitment on the CAR-E elements.

A. and B. *IWS1 phosphorylation controls Prp19 recruitment on CAR-E elements.* RIP assays in NCI-H522 and NCI-H1299 cells transduced with the indicated constructs, show that whereas the binding of Prp19 to the CAR-E elements depends on the phosphorylation of IWS1, the binding of U2AF65 does not. The bars show the mean fold enrichment in U2AF65 (upper) and Prp19 (lower panel) binding in the indicated regions (anti-U2AF65 or anti-Prp19 IP, vs IgG control IP) ± SD. Data were normalized relative to the input (2%). The primer location within the intronless genes is described in Figure S4A.

C. *IWS1 phosphorylation regulates the nucleocytoplasmic export of intronless mRNAs in patients with Lung Adenocarcinoma. (*Upper panel) Western blots of lysates of 6 human LUAD samples with high and low IWS1 expression, as previously identified (Laliotis et al., 2020[15]), were probed with anti-IWS1, anti-p-IWS1 and anti-β-actin (control) antibodies. (first three lanes). RT-PCR of *U2AF2*, using oligonucleotide primers that map in exons 1 and 3 (forth lane). (Lower Panel) LUAD tumor samples were fractionated into cytoplasmic and nuclear fractions. *IFNA1, IFNB1, JUN, HSPB3* and *GAPDH* mRNA levels in each fraction were determined using qRT–PCR. For each transcript, values are represented as cytoplasmic to nuclear ratios and were normalized to 18S rRNA. The accuracy of the fractionation was validated with the experiment in Figure S4B. Bars show the mean normalized Cytosolic/Nuclear ratio ±SD

D. *IWS1 phosphorylation controls Prp19 recruitment on CAR-E in patients with Lung Adenocarcinoma.* RIP assays in the same high and low-IWS1 group, show that whereas the binding of Prp19 to the CAR-E elements depends on the phosphorylation of IWS1, the binding of U2AF65 does not. The bars show the mean fold enrichment in U2AF65 (upper) and Prp19 (lower panel) binding in the indicated regions (anti-U2AF65 or anti-Prp19 IP, vs IgG control IP) ± SD. Data were normalized relative to the input (2%).

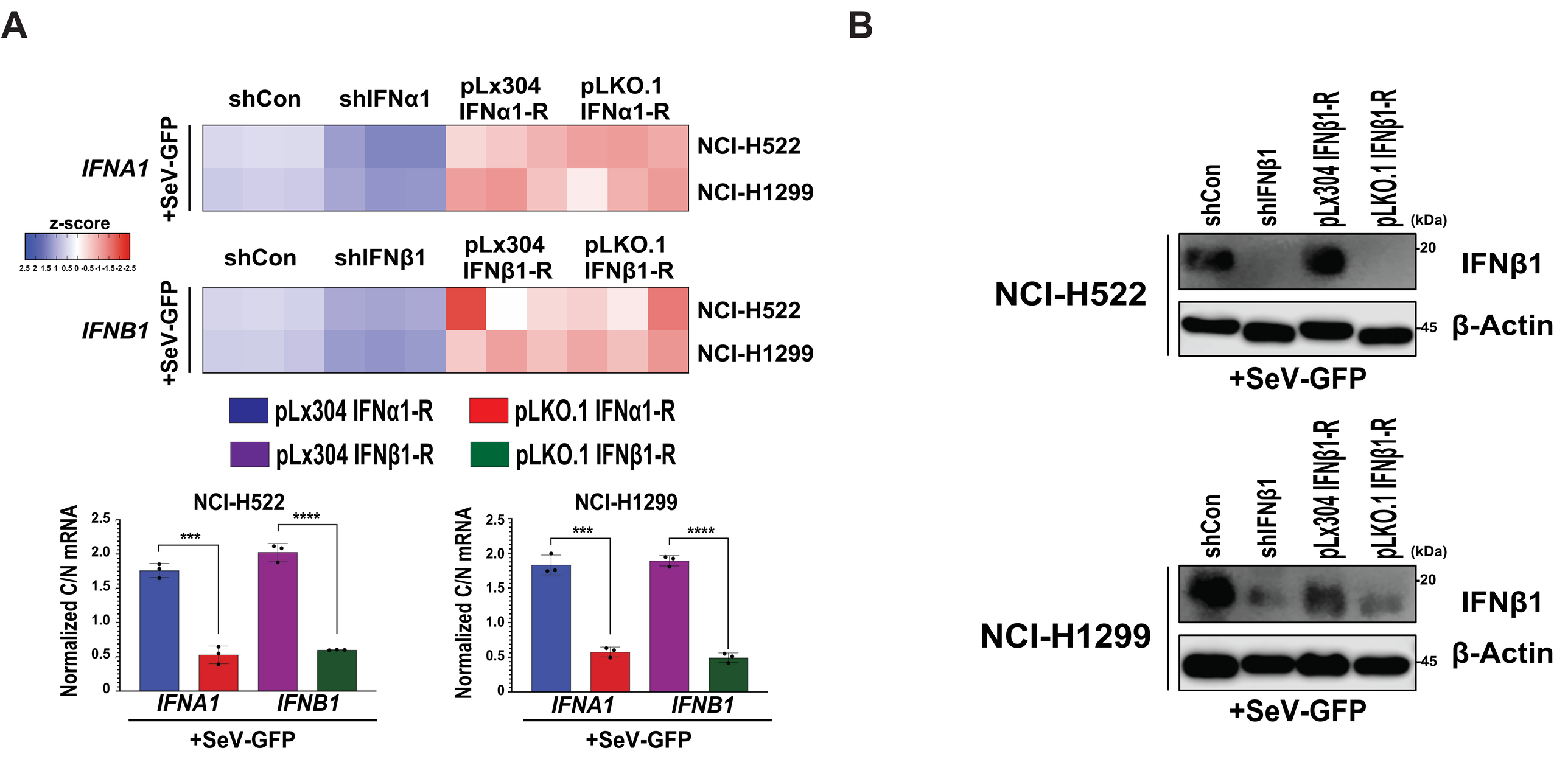
A
shCon
shIFNα1
pLx304 IFNα1-R
pLKO.1 IFNα1-R
IFNA1
+SeV-GFP
NCI-H522
NCI-H1299
z-score
2.5 2 1.5 1 0.5 0 -0.5 -1 -1.5 -2 -2.5
shCon
shIFNβ1
pLx304 IFNβ1-R
pLKO.1 IFNβ1-R
IFNB1
+SeV-GFP
NCI-H522
NCI-H1299
pLx304 IFNα1-R
pLKO.1 IFNα1-R
pLx304 IFNβ1-R
pLKO.1 IFNβ1-R
NCI-H522
Normalized C/N mRNA
2.5
2.0
1.5
1.0
0.5
0
***
****
IFNA1
IFNB1
+SeV-GFP
NCI-H1299
Normalized C/N mRNA
2.5
2.0
1.5
1.0
0.5
0
***
****
IFNA1
IFNB1
+SeV-GFP
B
shCon
shIFNβ1
pLx304 IFNβ1-R
pLKO.1 IFNβ1-R
(kDa)
NCI-H522
20
IFNβ1
45
β-Actin
+SeV-GFP
shCon
shIFNβ1
pLx304 IFNβ1-R
pLKO.1 IFNβ1-R
(kDa)
NCI-H1299
20
IFNβ1
45
β-Actin
+SeV-GFP

Figure 5. RNA-Pol II affects the splicing-independent nuclear export of intronless genes.

A. *RNA Pol II contributes to the nucleocytoplasmic export of intronless genes* (Upper panel) Total RNA was harvested from NCI-H522 and NCI-H1299 cells, transduced with the indicated constructs. The construct maps for the pLx304 (RNA Pol II-driven) or pLKO.1 (RNA Pol III-driven) can be found in Fig. S5A. The expression of *IFNA1 and IFNB1,* mRNAs was determined by qRT-PCR and normalized to 18S rRNA levels. The results are represented as heatmap using z-scores from three individual biological experiments. For type I IFN induction SeV infection was performed. (Lower panel) The same cells were fractionated into cytoplasmic and nuclear fractions, *IFNA1, IFNB1* and *GAPDH* mRNA levels in each fraction were determined using qRT–PCR. For each transcript, values are represented as cytoplasmic to nuclear ratios and were normalized to 18S rRNA. For type I IFN induction SeV-GFP infection was performed. The accuracy of the fractionation was validated with the experiment in Figure S5B. Bars show the mean normalized Cytosolic/Nuclear ratio ±SD

B. Western blots of lysates of NCI-H522 and NCI-H1299 cells, transduced with the indicated constructs, were probed with anti-IFNβ1 and anti-β-actin (control) antibodies. For type I IFN induction SeV-GFP infection was performed. In this figure, NCI-H522 and NCI-H1299 cells were infected with MOI of 0.5 for 16h and MOI of 0.25 for 24h of SeV-GFP virus, respectively. All assays in this figure were done in triplicate, on three biological replicates. n.s : non-significant *$p<0.05$, **$p<0.01$, ***$p<0.001$, ****$p<0.0001$. (one-side unpaired t-test).

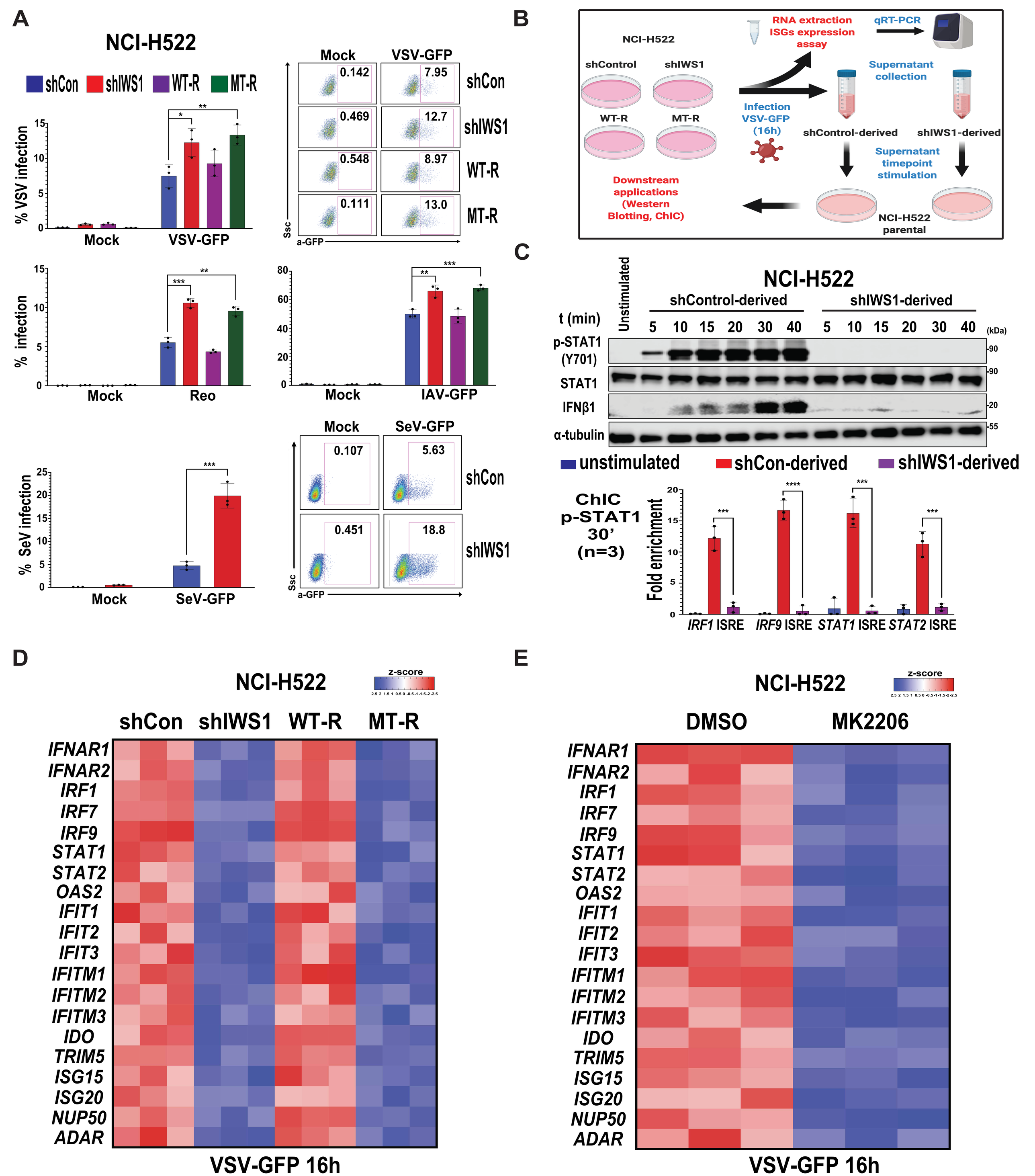
A
NCI-H522
shCon
shIWS1
WT-R
MT-R
% VSV infection
Mock
VSV-GFP
Mock
VSV-GFP
0.142
7.95
0.469
12.7
0.548
8.97
0.111
13.0
Ssc
a-GFP
% infection
Mock
Reo
Mock
IAV-GFP
% SeV infection
Mock
SeV-GFP
Mock
SeV-GFP
0.107
5.63
0.451
18.8
B
NCI-H522
shControl
shIWS1
WT-R
MT-R
RNA extraction
ISGs expression
assay
qRT-PCR
Supernatant
collection
Infection
VSV-GFP
(16h)
shControl-derived
shIWS1-derived
Supernatant
timepoint
stimulation
Downstream
applications
(Western
Blotting, ChIC)
NCI-H522
parental
C
NCI-H522
Unstimulated
shControl-derived
shIWS1-derived
t (min)
5 10 15 20 30 40
5 10 15 20 30 40
(kDa)
p-STAT1
(Y701)
STAT1
IFNβ1
α-tubulin
unstimulated
shCon-derived
shIWS1-derived
ChIC
p-STAT1
30'
(n=3)
Fold enrichment
IRF1 ISRE
IRF9 ISRE
STAT1 ISRE
STAT2 ISRE
D
NCI-H522
z-score
shCon
shIWS1
WT-R
MT-R
IFNAR1
IFNAR2
IRF1
IRF7
IRF9
STAT1
STAT2
OAS2
IFIT1
IFIT2
IFIT3
IFITM1
IFITM2
IFITM3
IDO
TRIM5
ISG15
ISG20
NUP50
ADAR
VSV-GFP 16h
E
NCI-H522
z-score
DMSO
MK2206
IFNAR1
IFNAR2
IRF1
IRF7
IRF9
STAT1
STAT2
OAS2
IFIT1
IFIT2
IFIT3
IFITM1
IFITM2
IFITM3
IDO
TRIM5
ISG15
ISG20
NUP50
ADAR
VSV-GFP 16h

Figure 6. The loss of IWS1 phosphorylation enhances viral infection, through the aberrant p-STAT1 signaling and transcription of ISGs.

A. *The loss of IWS1 phosphorylation enhances viral replication.* The indicated NCI-H522 cells were infected with VSV-GFP, SeV-GFP, Reovirus or Influenza A-GFP at an MOI of 0.5 for 16 hours (VSV-GFP and IAV-GFP), MOI of 1 for 24h hours (SeV-GFP and Reovirus), respectively. Cells were then fixed and were examined for GFP positivity (for VSV, SeV and Flu) to measure the percentage of cells infected using flow cytometry. For Reovirus, the fixed-infected cells were stained with anti-reovirus antibody, followed by anti-mouse Alexa488-conjugated secondary antibody, and analyzed as well with Flow cytometry. Results shown are representative of at least three independent experiments, each performed with triplicate samples. Bars show the % infection of each viral strain ±SD.

B. *Summary of the experimental design.* NCI-H522 shControl, shIWS1, shIWS1/WT-R and shIWS1/MT-R cells were infected with VSV-GFP at an MOI of 0.5 for 16h. Then the cells were harvested for RNA and their supernatant was collected. The RNA was used for downstream qRT-PCR applications. The supernatant derived from shControl and shIWS1 was used to stimulate NCI-H522 parental cells in time point intervals. These cells were used for Chromatin Immuno Cleavage (ChIC) or were harvested for protein.

C. *Loss of IWS1 phosphorylation impairs p-STAT1 activation following viral infection.* (Upper panel) NCI-H522 parental cells were stimulated for the indicated time point intervals with shControl and shIWS1-derived supernatant and were harvested for protein. In parallel experiments, NCI-H522 unstimulated parental cells were harvested as control. The protein lysates were probed with the indicated antibodies. (Lower panel) ChIC assays showing the binding of p-STAT1 in the *ISRE of IRF1, IRF9, STAT1 and STAT2* genes, in NCI-H522 cells following stimulation for 30' with shControl and shIWS1-derived supernatant. In parallel experiments, NCI-

H522 unstimulated parental cells were proceeded as control. The bars show the mean fold enrichment in p-STAT1 binding in the indicated regions ±SD, relative to IgG IP.

D. *Loss of AKT/p-IWS1 axis impairs the ISG transcription following viral infection.* Total RNA was harvested from NCI-H522 cells, transduced with the indicated constructs following VSV-GFP infection at MOI 0.5 for 16h. The expression of 20 ISGs mRNAs was determined by qRT-PCR and normalized to 18S rRNA. The results are represented as heatmap using z-scores from three individual biological experiments.

E. Total RNA was harvested from NCI-H522 cells, treated with DMSO or 5μM of the pan-AKT inhibitor MK2206, following VSV-GFP infection at MOI x for 16h. The expression of 20 ISGs mRNAs was determined by qRT-PCR and normalized to 18S rRNA. The results are represented as heatmap using z-scores from three individual biological experiments. All assays in this figure were done in triplicate, on three biological replicates. n.s : non-significant *$p<0.05$, **$p<0.01$, ***$p<0.001$, ****$p<0.0001$. (one-side unpaired t-test).

A

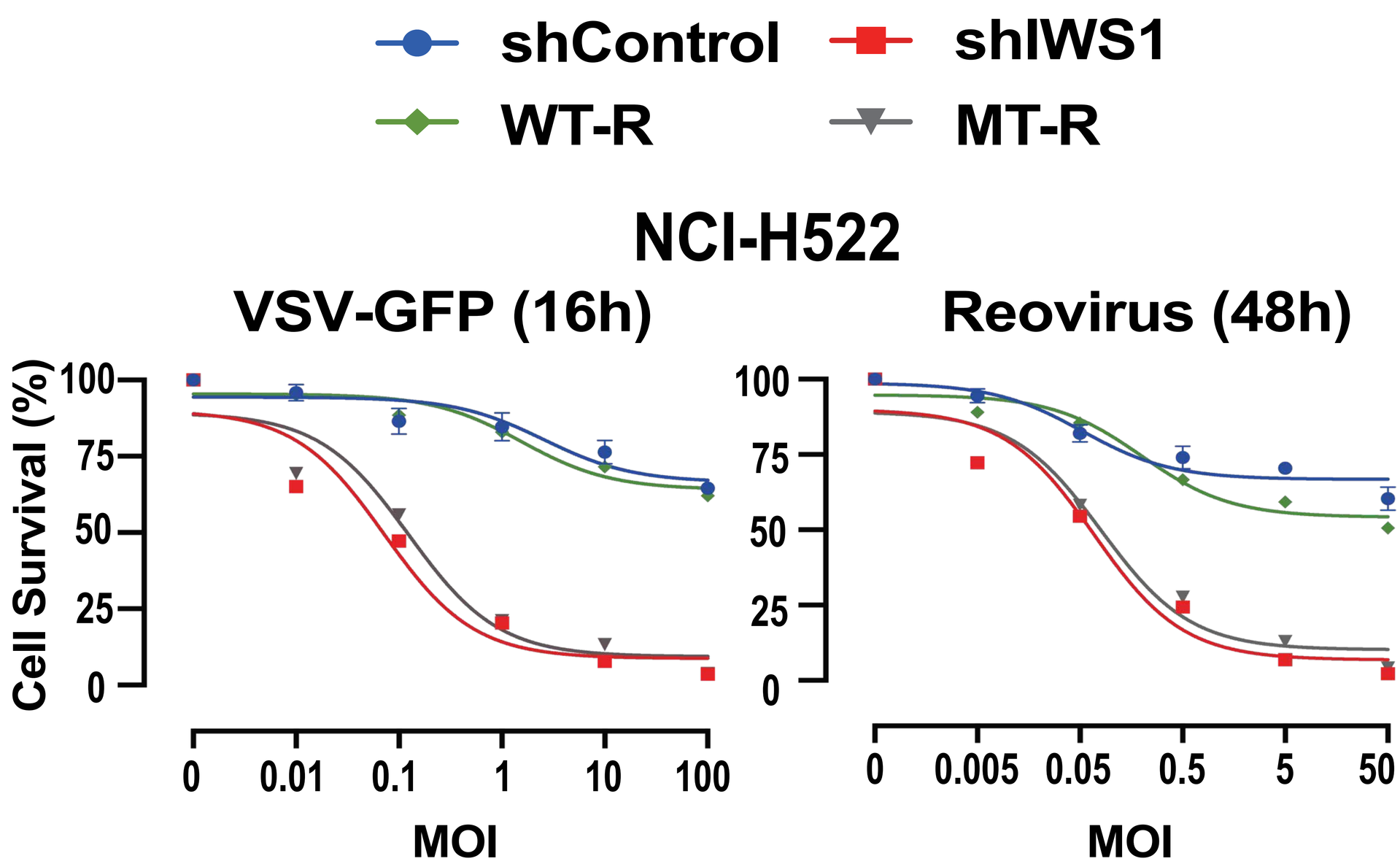
shControl
shIWS1
WT-R
MT-R
NCI-H522
VSV-GFP (16h)
Reovirus (48h)
Cell Survival (%)
100
75
50
25
0
0
0.01
0.1
1
10
100
MOI
0
0.005
0.05
0.5
5
50
MOI

B

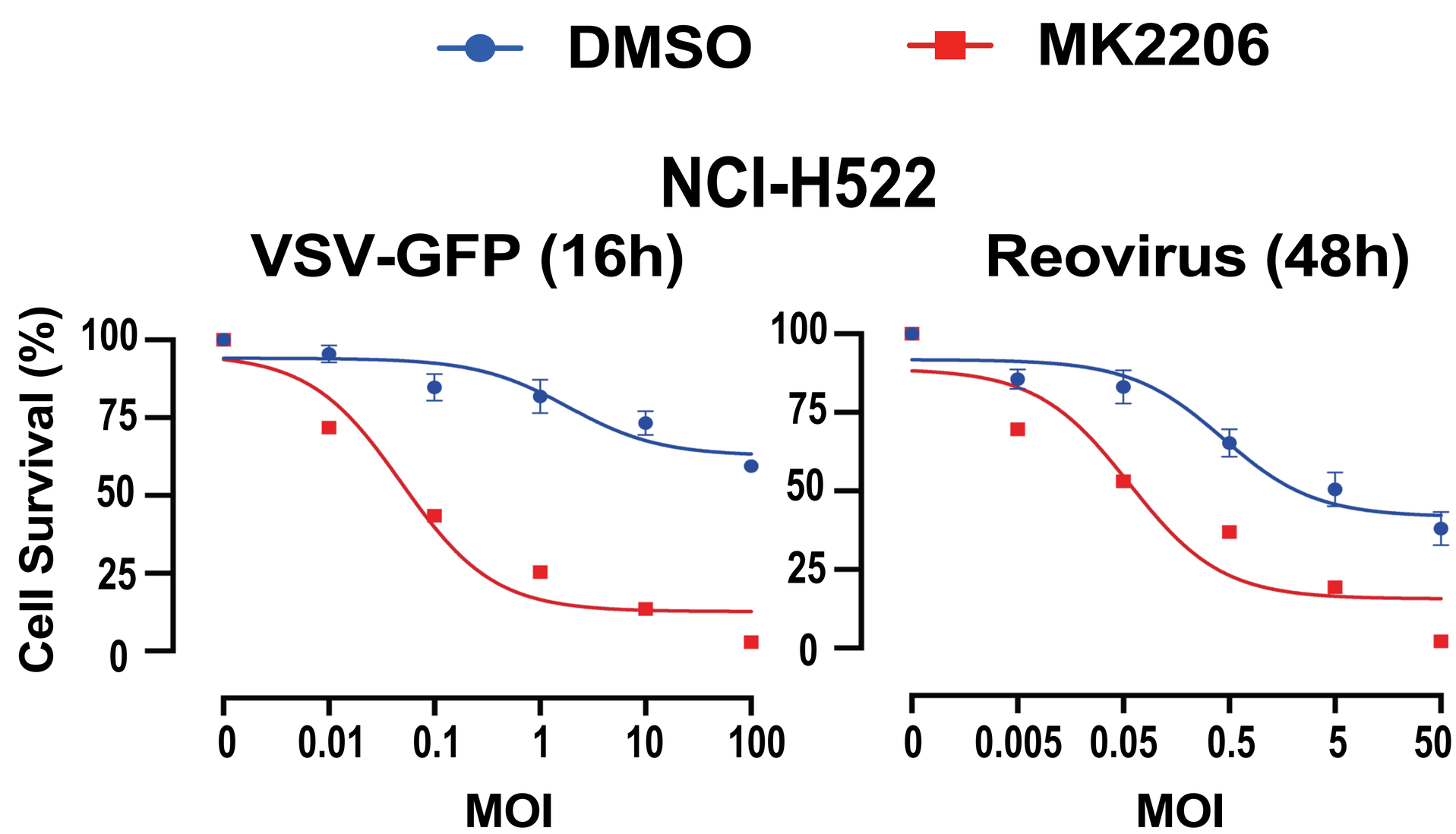
DMSO
MK2206
NCI-H522
VSV-GFP (16h)
Reovirus (48h)
Cell Survival (%)
100
75
50
25
0
0
0.01
0.1
1
10
100
MOI
0
0.005
0.05
0.5
5
50
MOI

C

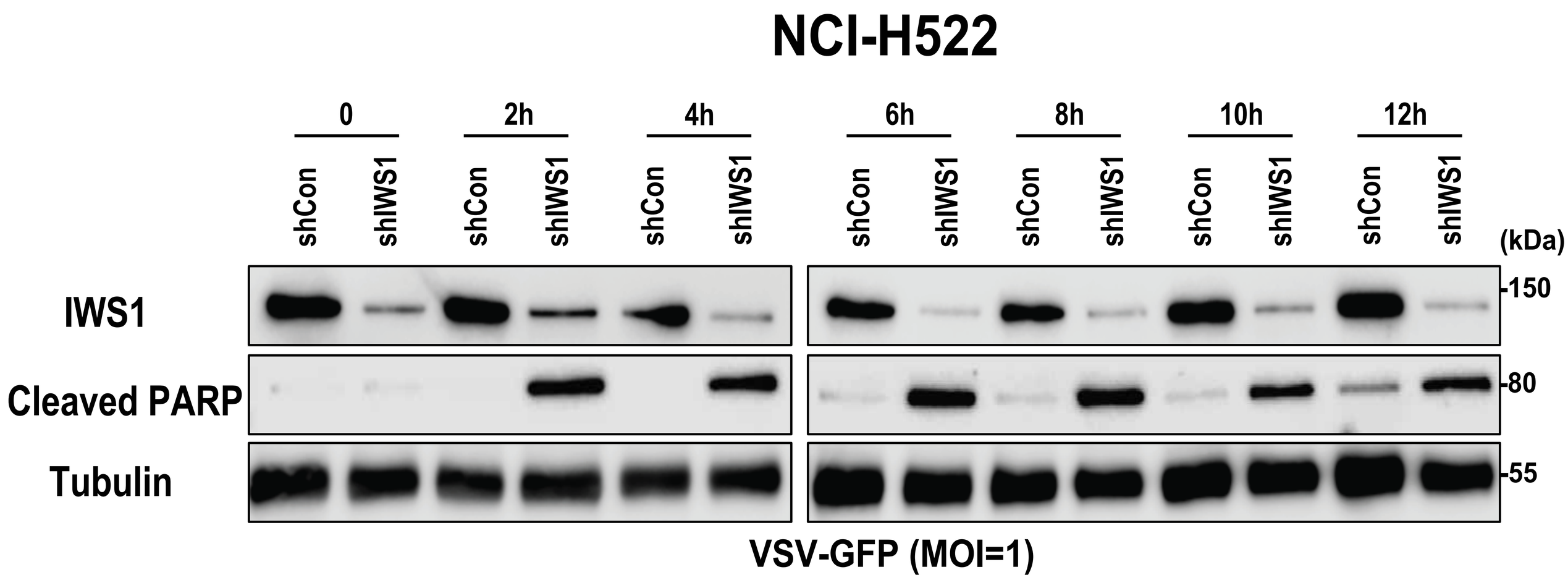
NCI-H522
0
2h
4h
6h
8h
10h
12h
shCon
shIWS1
(kDa)
IWS1
Cleaved PARP
Tubulin
150
80
55
VSV-GFP (MOI=1)

Figure 7. Inhibition of the AKT/p-IWS1 axis sensitizes lung adenocarcinoma cells to oncolytic viral killing.

A. *The loss of IWS1 phosphorylation sensitizes lung adenocarcinoma cells to oncolytic viral killing.* NCI-H522 cells transduced with the indicated constructs were exposed to increasing MOI of VSV-GFP or Reovirus for 16h and 48h, respectively. Cell proliferation was assessed by fluorescent detection of the reduction of resazurin to resorufin by viable cells and expressed as a percentage of uninfected cells. Mean values are shown ±SD (n=3) and data are representative of two independent experiments.

B. *The loss of AKT/p-IWS1 axis sensitizes lung adenocarcinoma cells to oncolytic viral killing.* NCI-H522 cells treated with DMSO or 5μM of the pan-AKT inhibitor MK2206, were exposed to increasing MOI of VSV-GFP or Reovirus for 16h and 48h, respectively. Cell proliferation was assessed by fluorescent detection of the reduction of resazurin to resorufin by viable cells and expressed as a percentage of uninfected cells. Mean values are shown ±SD (n=3) and data are representative of two independent experiments.

C. *The loss of IWS1 phosphorylation sensitizes lung adenocarcinoma cells to oncolytic viral killing via Caspase-mediated death.* NCI-H522 shControl and shIWS1 cells were infected for the indicated time point intervals with VSV-GFP at a MOI=1. Western blot lysates from these time points were probed with the indicated antibodies, showing a robust cleavage of PARP, a sensitive marker of Caspase mediated apoptosis, in shIWS1 cells even in early time points of infections.

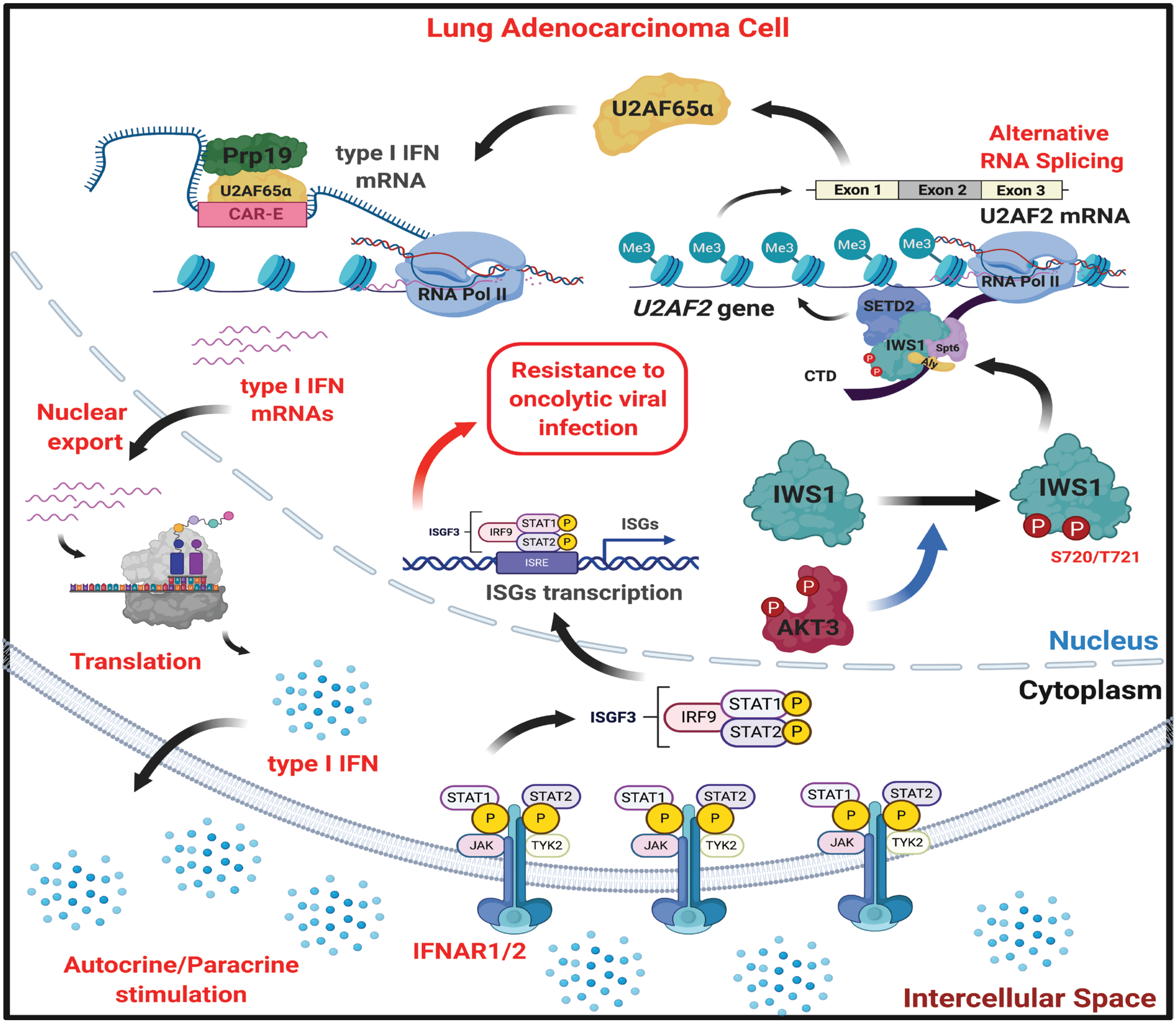
Lung Adenocarcinoma Cell
U2AF65α
Prp19
U2AF65α
CAR-E
type I IFN
mRNA
RNA Pol II
Alternative
RNA Splicing
Exon 1
Exon 2
Exon 3
U2AF2 mRNA
Me3
U2AF2 gene
SETD2
IWS1
Spt6
Aly
CTD
RNA Pol II
Resistance to
oncolytic viral
infection
type I IFN
mRNAs
Nuclear
export
IWS1
IWS1
S720/T721
AKT3
ISGF3
IRF9
STAT1
STAT2
ISRE
ISGs
ISGs transcription
Nucleus
Translation
Cytoplasm
ISGF3
IRF9
STAT1
STAT2
type I IFN
STAT1
STAT2
JAK
TYK2
IFNAR1/2
Autocrine/Paracrine
stimulation
Intercellular Space

Figure 8. Model of the effect of IWS1 phosphorylation at S720/721, on type I IFN expression and response to oncolytic viral infection.

Model of the effect of IWS1 phosphorylation at S720/721, on type I IFN expression and response to oncolytic viral infection. The phosphorylation of IWS1 at S720/T721 by AKT kinase controls the epigenetic regulation of *U2AF2* alternative RNA splicing, leading to inclusion of exon 2 in the mature *U2AF2* mRNA. Subsequently, the U2AF65α isoform binds CAR-E of type I IFNs and recruits Prp19, promoting their nucleocytoplasmic export and expression. During oncolytic viral infection, type I IFNs are properly exported, expressed and by acting in an autocrine and paracrine fashion, stimulate the IFNAR1/2 receptor. The latter leads to p-STAT1 activation and assembly of the ISGF3 on ISGs promoters. This confers resistance of lung adenocarcinoma cells to oncolytic viral infection.

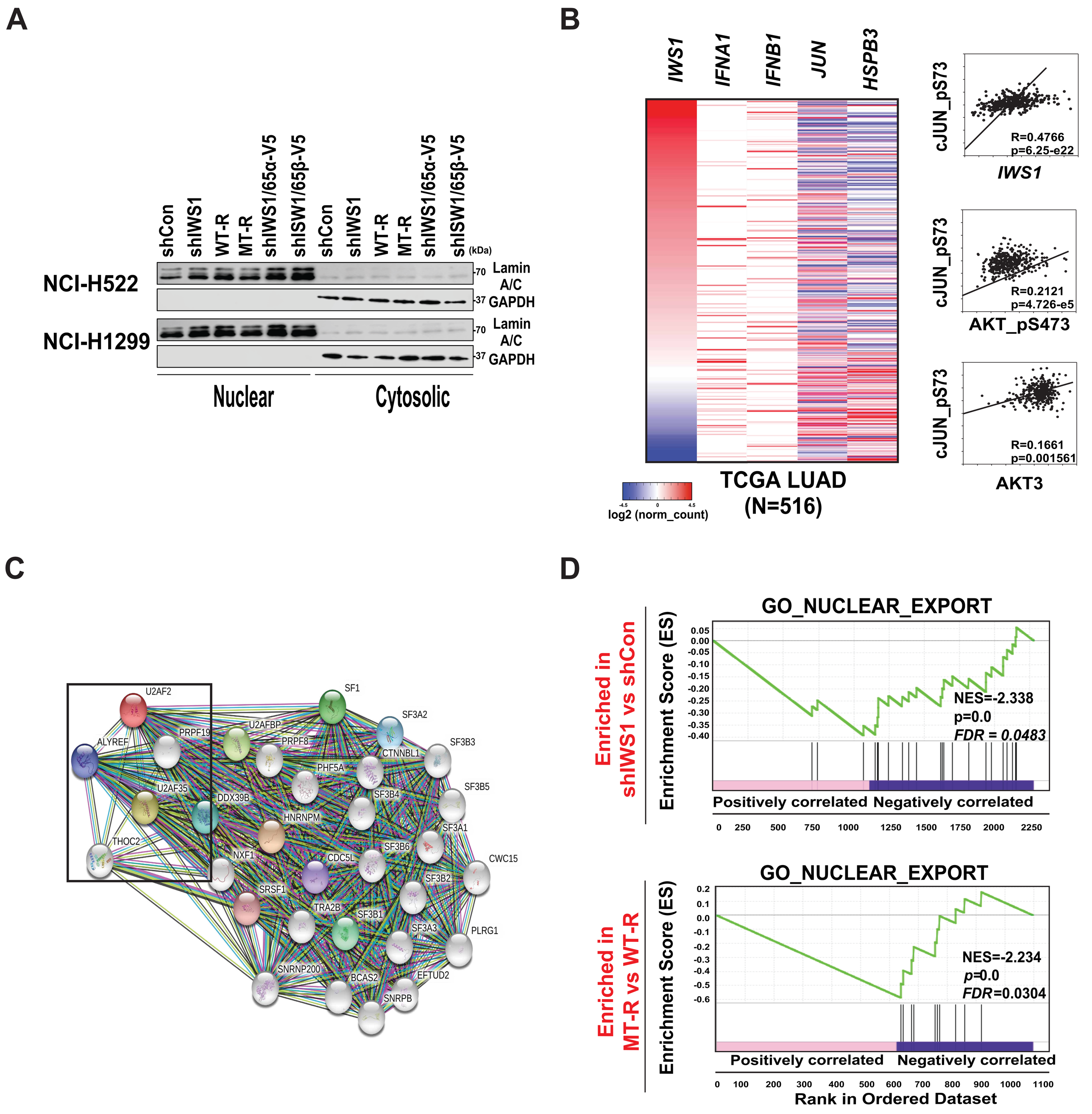
A
shCon
shIWS1
WT-R
MT-R
shIWS1/65α-V5
shISW1/65β-V5
(kDa)
NCI-H522
NCI-H1299
70
37
Lamin A/C
GAPDH
Nuclear
Cytosolic
B
IWS1
IFNA1
IFNB1
JUN
HSPB3
TCGA LUAD
(N=516)
log2 (norm_count)
-4.5
0
4.5
cJUN_pS73
IWS1
R=0.4766
p=6.25-e22
AKT_pS473
R=0.2121
p=4.726-e5
AKT3
R=0.1661
p=0.001561
C
U2AF2
SF1
SF3A2
U2AFBP
PRPF19
ALYREF
PRPF8
SF3B3
CTNNBL1
PHF5A
U2AF35
SF3B5
DDX39B
SF3B4
HNRNPM
SF3A1
THOC2
SF3B6
NXF1
CDC5L
CWC15
SF3B2
SRSF1
TRA2B
SF3B1
SF3A3
PLRG1
SNRNP200
BCAS2
EFTUD2
SNRPB
D
GO_NUCLEAR_EXPORT
Enriched in shIWS1 vs shCon
Enrichment Score (ES)
NES=-2.338
p=0.0
FDR = 0.0483
Positively correlated
Negatively correlated
GO_NUCLEAR_EXPORT
Enriched in MT-R vs WT-R
Enrichment Score (ES)
NES=-2.234
p=0.0
FDR=0.0304
Positively correlated
Negatively correlated
Rank in Ordered Dataset

Figure S1 (relative to Figure 1). IWS1 phosphorylation regulates the nucleocytoplasmic transport of mRNAs transcribed from a set of intronless genes, via *U2AF2* alternative RNA splicing.

A. The cytosolic and nuclear compartment of the indicated NCI-H522 (upper two lines) and NCI-H1299 cells (lower two lines) were probed with the indicated antibodies, to validate the fractionation.

B. (Left panel) Heat Maps showing the correlation of IWS1 RNA levels with intronless genes in the TCGA LUAD database. The RNA-seq expression values from each individual patient were expressed as $\log_2$ normalized counts and they were used to calculate the correlation coefficients. (Right panel) Correlation coefficient graphs of Reverse Phase Protein Assay (RPPA) levels of p-c-Jun (S73) in TCGA LUAD with the RNA levels of IWS1 (top), RRPA levels p-AKT (S473) (middle) and RNA levels of AKT3 (lower).

C. The Protein-Protein Interaction (PPI) network analysis of U2AF65-Prp19 using the STRING database. U2AF65 and Prp19 interact with components of TREX complex and Ref/Aly controlling the export of naturally intronless genes (red box)

D. Gene Set Enrichment Analysis (GSEA) of genes differentially expressed in shIWS1 versus shControl (left panels) and in shIWS1/MT-R versus shIWS1/WT-R (right panels) NCI-H522 cells demonstrates significant enrichment in genes involved in Nuclear Export. (NES–normalized enrichment score, FDR–false discovery ratio)

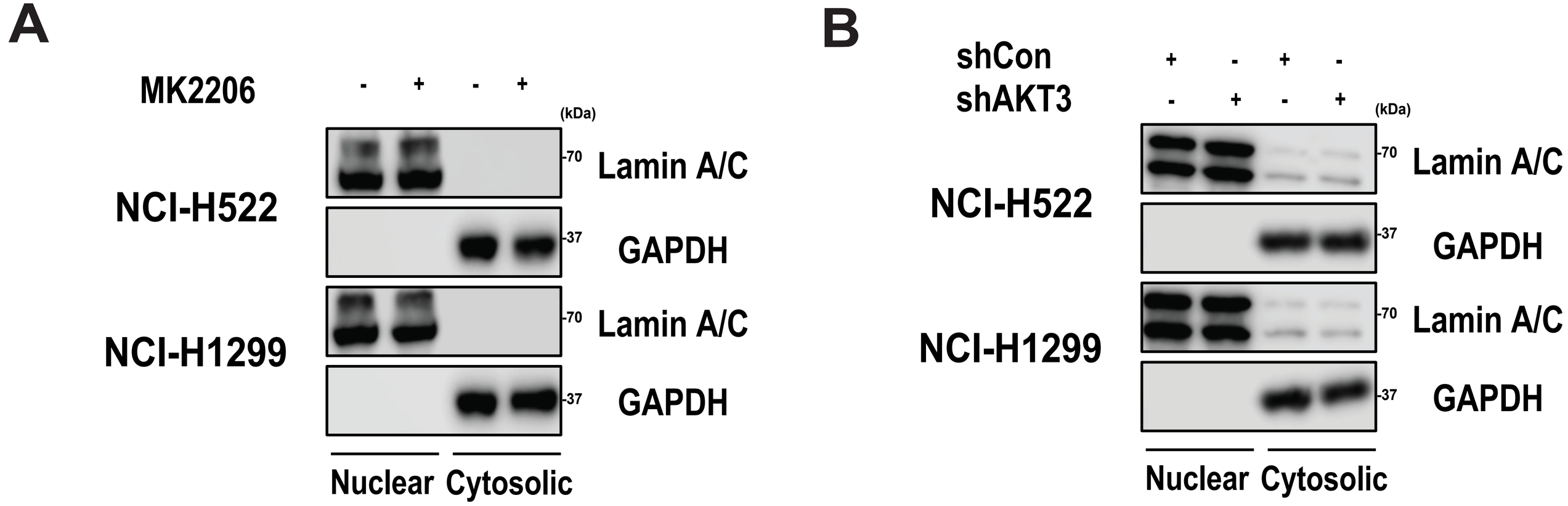
A
MK2206
- + - +
(kDa)
NCI-H522
-70
Lamin A/C
-37
GAPDH
NCI-H1299
-70
Lamin A/C
-37
GAPDH
Nuclear Cytosolic
B
shCon
shAKT3
+ - + -
- + - +
(kDa)
NCI-H522
-70
Lamin A/C
-37
GAPDH
NCI-H1299
-70
Lamin A/C
-37
GAPDH
Nuclear Cytosolic

Figure S2 (relative to Figure 2). AKT3 kinase affects the nucleocytoplasmic export of RNAs transcribed from intronless genes, thought IWS1 phosphorylation.

A and B. The cytosolic and nuclear compartment of the indicated NCI-H522 (upper two lines) and NCI-H1299 cells (lower two lines) were probed with the indicated antibodies, to validate the fractionation.

A

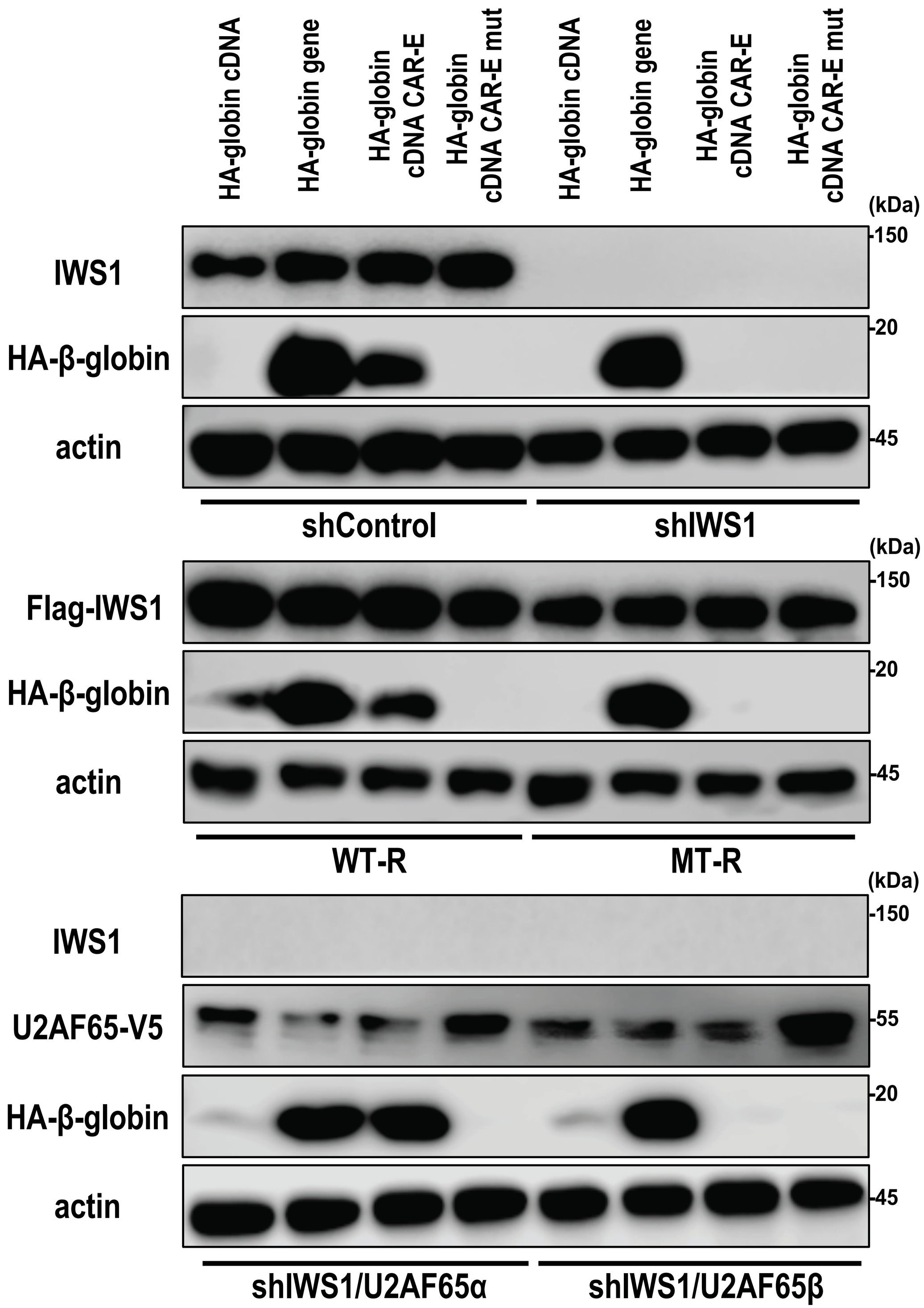
NCI-H1299
HA-globin cDNA
HA-globin gene
HA-globin cDNA CAR-E
HA-globin cDNA CAR-E mut
HA-globin cDNA
HA-globin gene
HA-globin cDNA CAR-E
HA-globin cDNA CAR-E mut
(kDa)
IWS1
150
HA-β-globin
20
actin
45
shControl
shIWS1
(kDa)
Flag-IWS1
150
HA-β-globin
20
actin
45
WT-R
MT-R
(kDa)
IWS1
150
U2AF65-V5
55
HA-β-globin
20
actin
45
shIWS1/U2AF65α
shIWS1/U2AF65β

Figure S3 (relative to Figure 3). IWS1 phosphorylation is required for the proper function of the CAR-E elements.

A. *IWS1 phosphorylation is required for CAR-E function.* NCI-H1299 cells transduced with the indicated constructs, were transfected transiently with pCMV HA-β-globin cDNA, HA-β-globin wt, HA-β-globin CAR-E and HA-β-globin CAR-E_{mut}. After 48h were harvested, and their lysates were probed with the indicated antibodies.

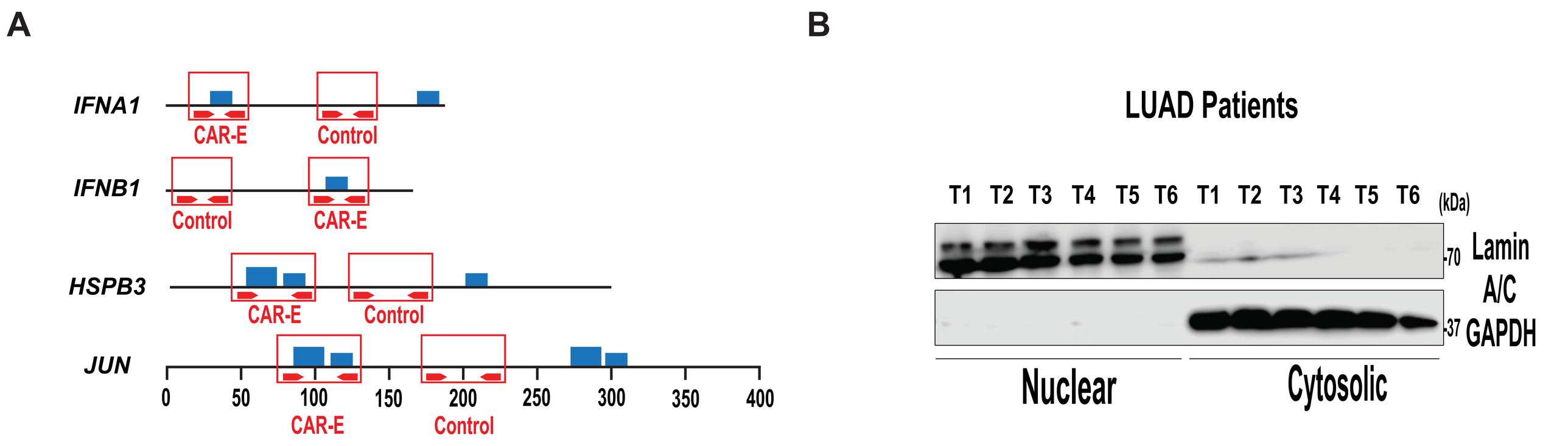
A
IFNA1
CAR-E
Control
IFNB1
Control
CAR-E
HSPB3
CAR-E
Control
JUN
0
50
100
150
200
250
300
350
400
CAR-E
Control
B
LUAD Patients
T1 T2 T3 T4 T5 T6 T1 T2 T3 T4 T5 T6
(kDa)
70
Lamin A/C
37
GAPDH
Nuclear
Cytosolic

Figure S4 (relative to Figure 4). The splicing of the *U2AF2* mRNA downstream of IWS1 phosphorylation, regulates the Prp19 recruitment on the CAR-E elements.

A. The 10-nt consensus element (CAR-E) identified in the CARs from *IFNα1, IFNβ1, c-Jun or HSPB3* is shown, as described previously (Lei et al., 2013[13]). The locations of the CAR-Es in each CAR are indicated by the boxes. The numbering is relative to the first nucleotide of each CAR sequence. In red boxes with the red arrows shows the primers used to amplify the CAR-E elements (CAR-E) or the control binding regions (Control) in the indicated genes.

B. The cytosolic and nuclear compartment of the indicated low and high-IWS1 LUAD group were probed with the indicated antibodies, to validate the fractionation.

A

CMV_promoter (RNA Pol II_driven)

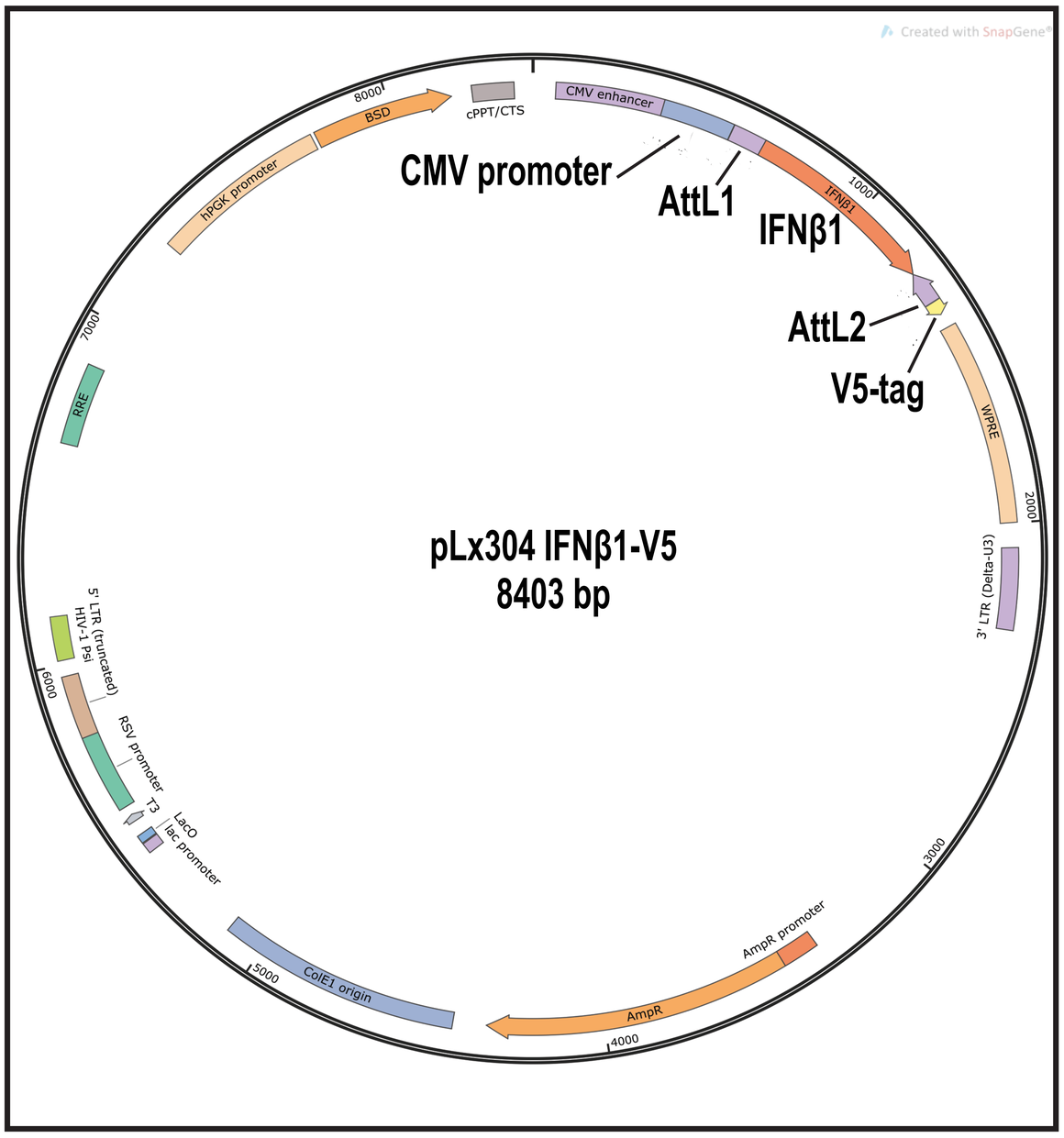

U6_promoter (RNA Pol III_driven)

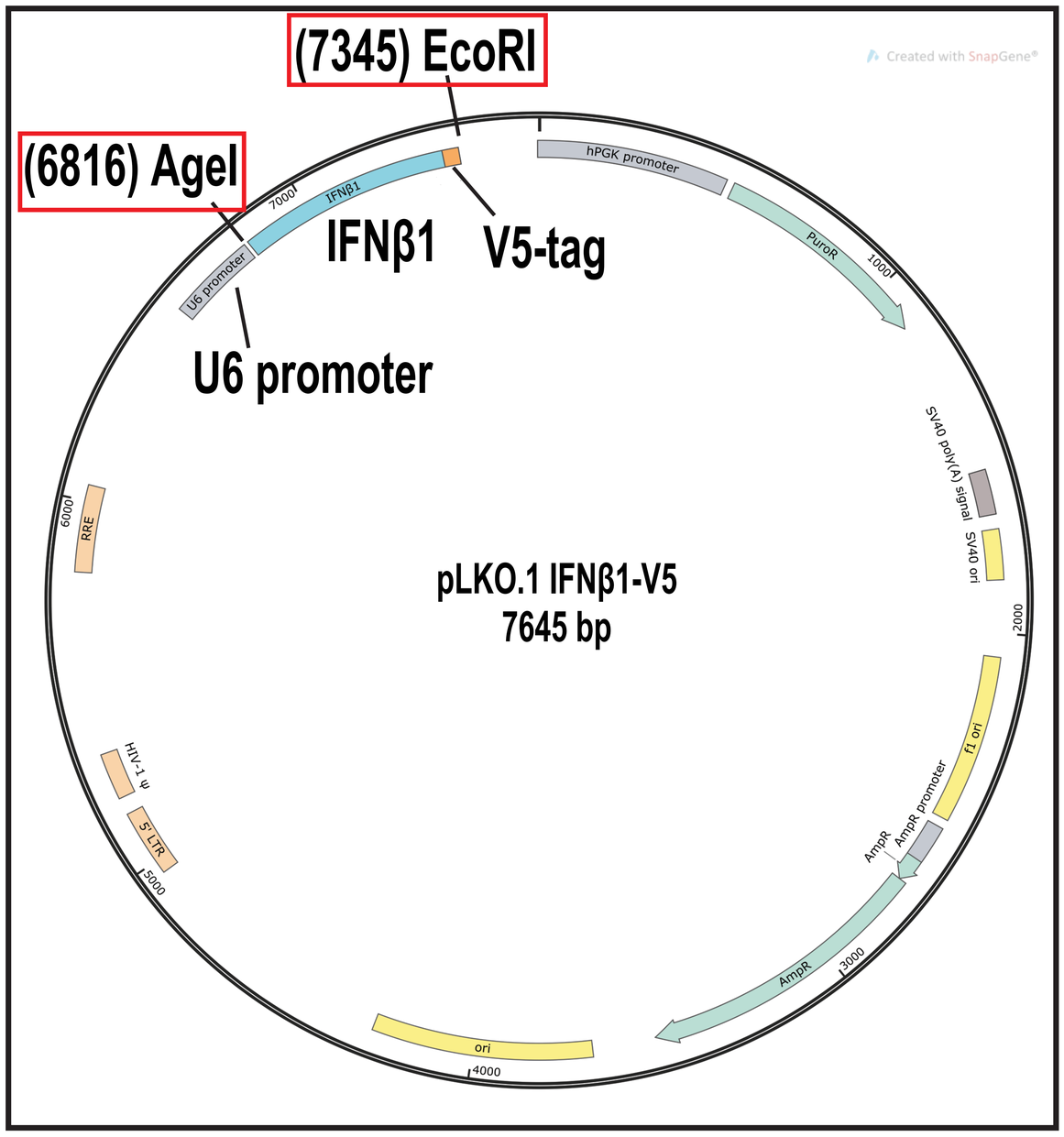

B

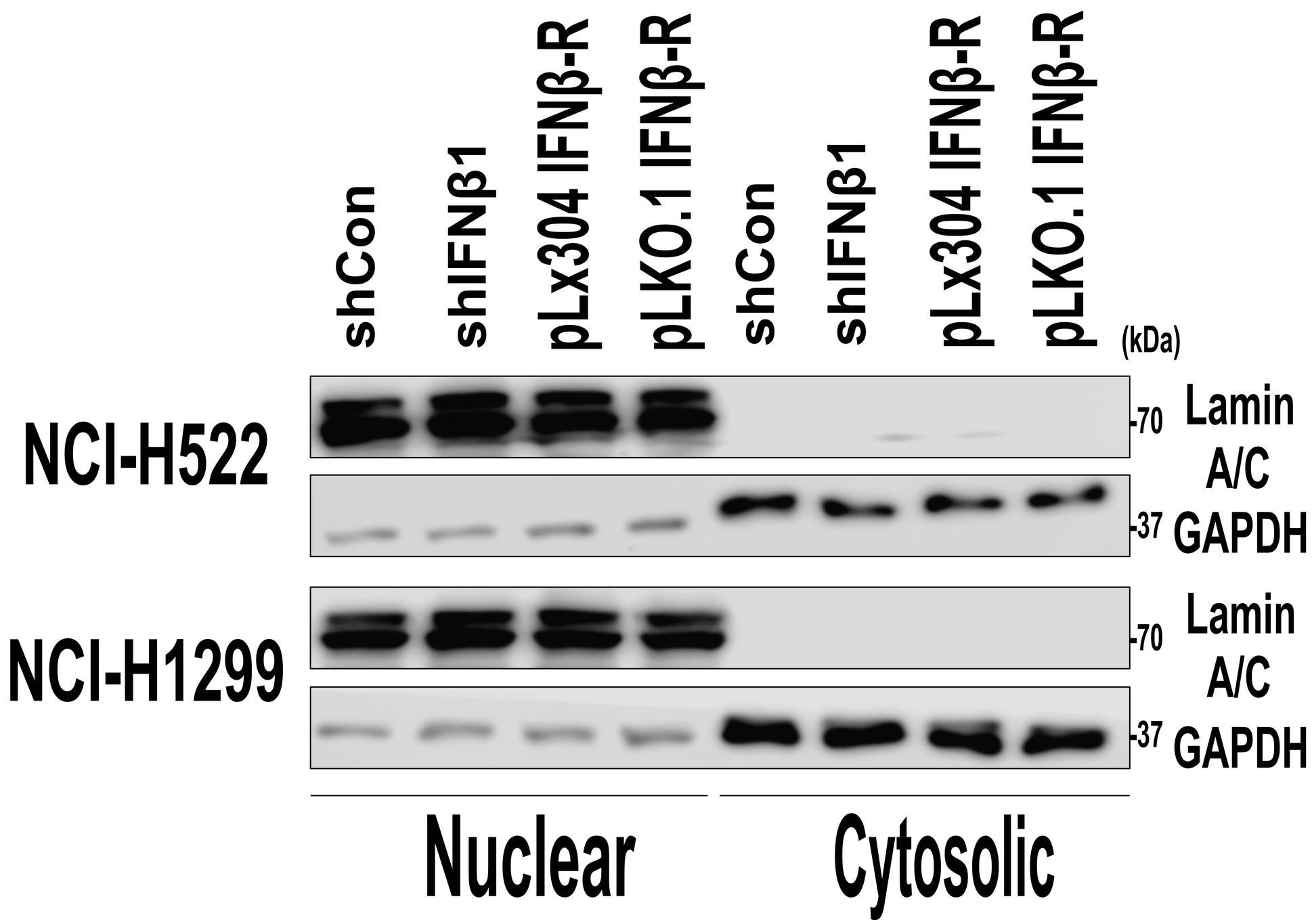

Figure S5 (relative to Figure 5). RNA-Pol II affects the splicing-independent nuclear export of intronless genes.

A. Schematic representation of CMV pLx304 IFNβ1-V5 (RNA Pol II-driven) and U6 pLKO.1 IFNβ1-V5 (RNA Pol III-driven) used in Fig. 5A and 5B is shown. The red boxes in pLx304 indicate the Gateway LR sites and in pLKO.1 map the restriction enzyme sites used for proper IFNβ1-V5 cloning into pLKO.1 (AgeI-EcoRI sites)

B. The cytosolic and nuclear compartment of the indicated NCI-H522 (upper two lines) and NCI-H1299 cells (lower two lines) were probed with the indicated antibodies, to validate the fractionation.

A

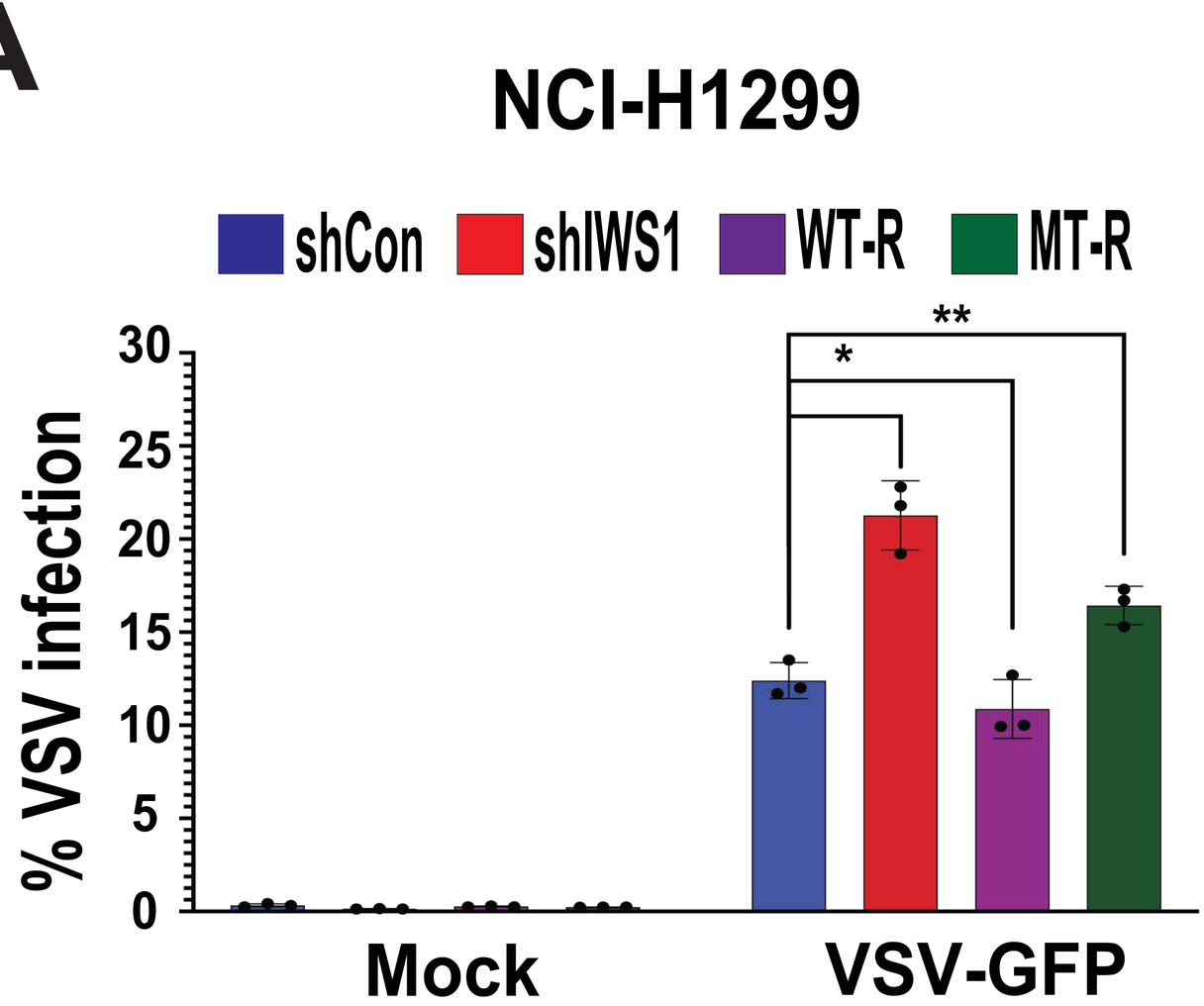
NCI-H1299
shCon
shIWS1
WT-R
MT-R
% VSV infection
30
25
20
15
10
5
0
*
**
Mock
VSV-GFP

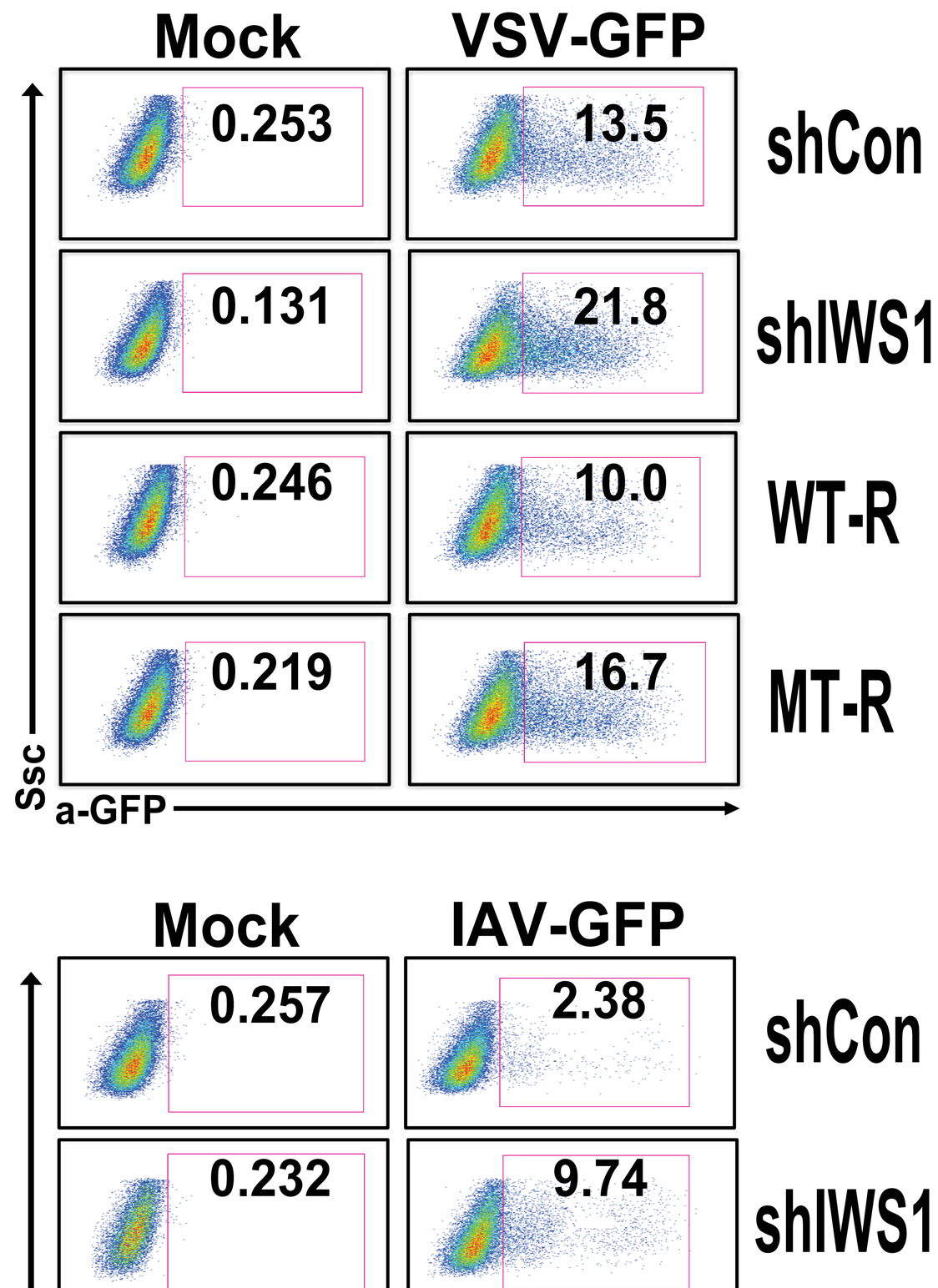
Mock
VSV-GFP
0.253
13.5
shCon
0.131
21.8
shIWS1
0.246
10.0
WT-R
0.219
16.7
MT-R
Ssc
a-GFP

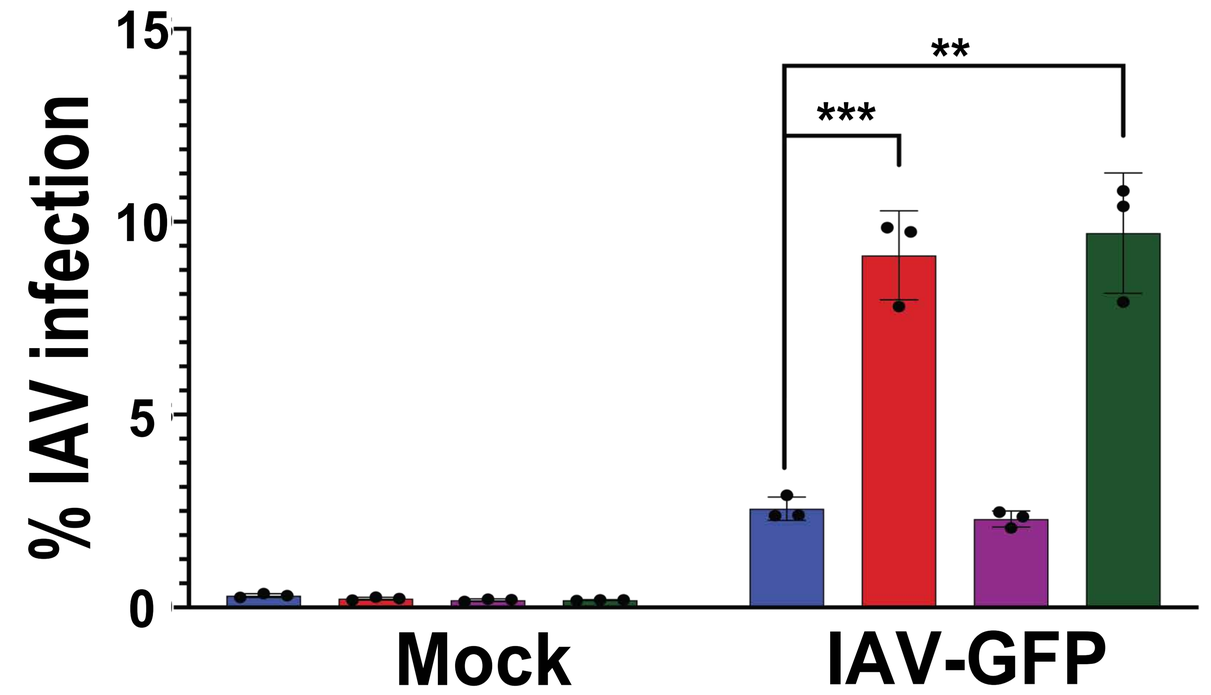
% IAV infection
15
10
5
0
***
**
Mock
IAV-GFP

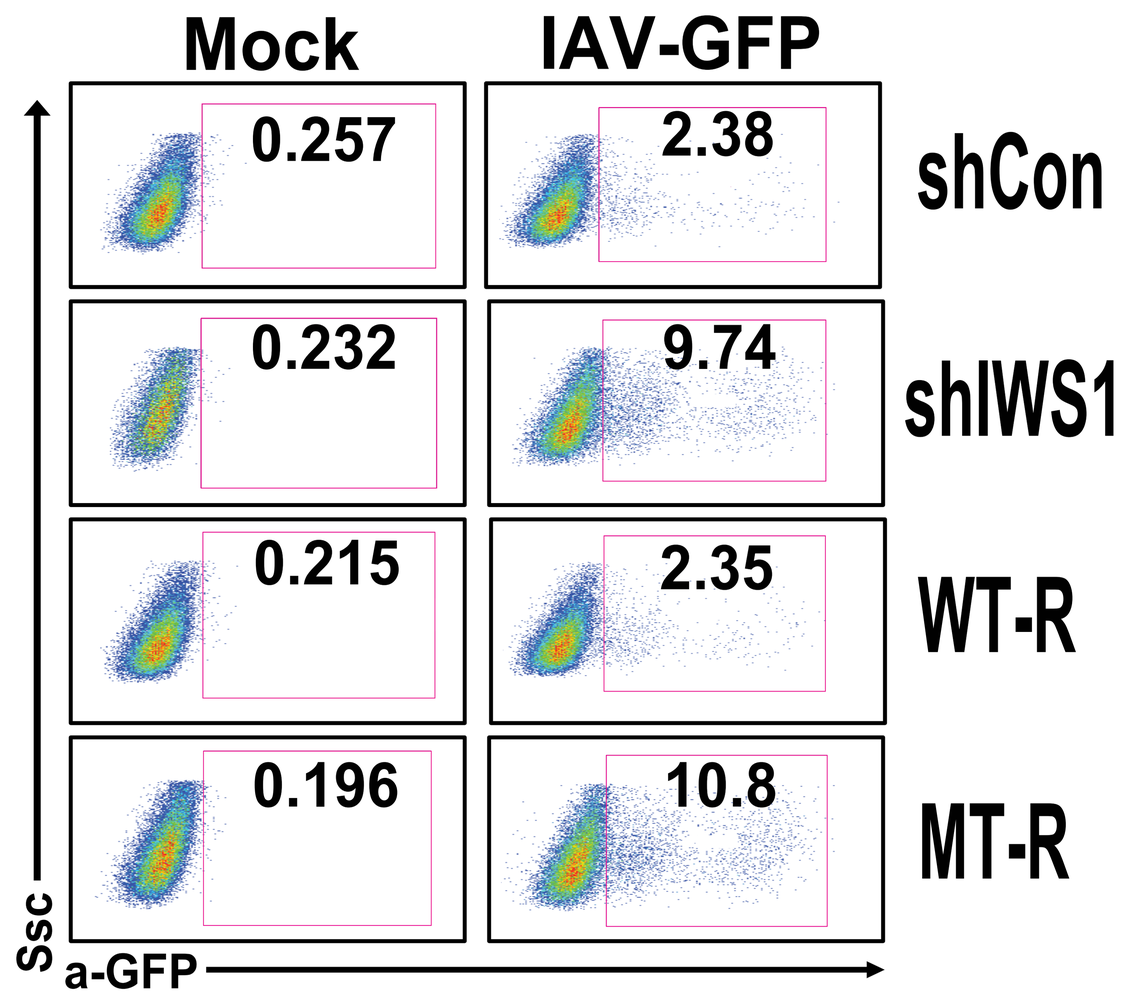
Mock
IAV-GFP
0.257
2.38
shCon
0.232
9.74
shIWS1
0.215
2.35
WT-R
0.196
10.8
MT-R
Ssc
a-GFP

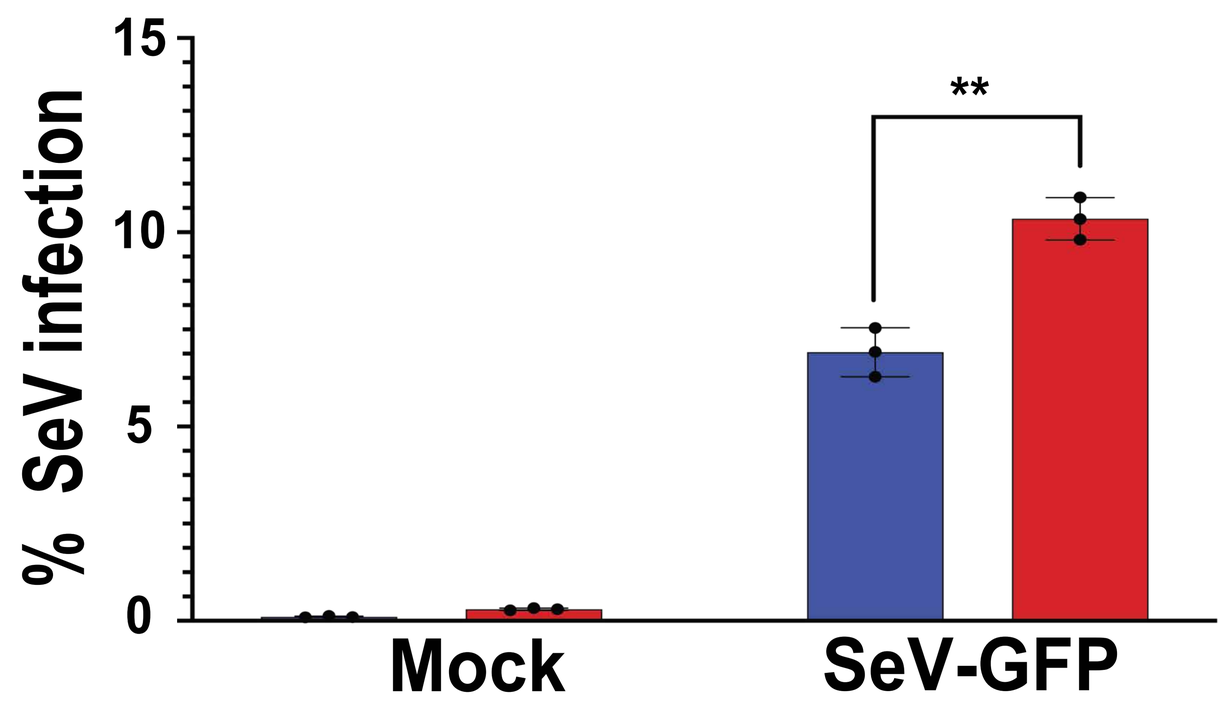
% SeV infection
15
10
5
0
**
Mock
SeV-GFP

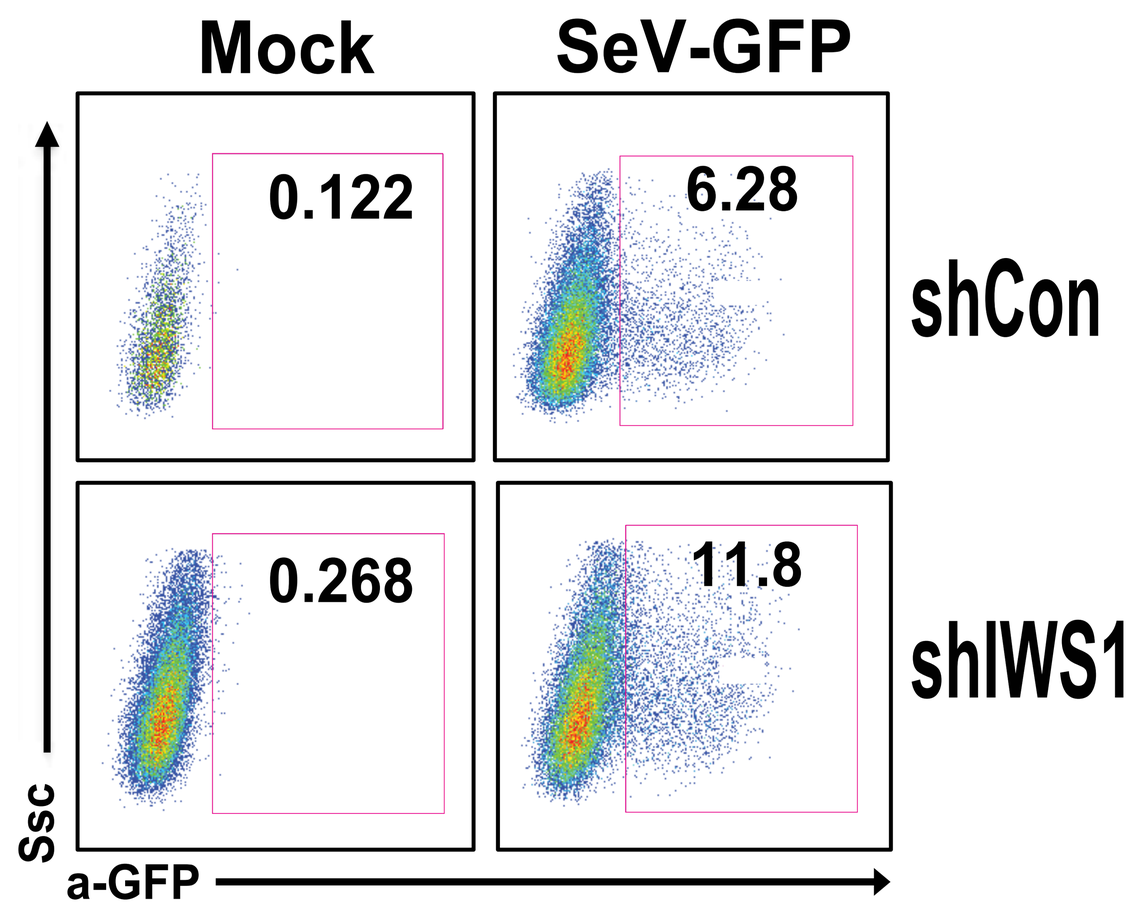
Mock
SeV-GFP
0.122
6.28
shCon
0.268
11.8
shIWS1
Ssc
a-GFP

B

IFNβ1 (1000U/mL)
Unstim.
5
10
15
20
30
40
IFNβ1
Tubulin
-20
-55
NCI-H522

Figure S6 (relative to Figure 6). The loss of IWS1 phosphorylation enhances viral replication, through the aberrant p-STAT1 signaling and transcription of ISGs.

A. *The loss of IWS1 phosphorylation enhances viral replication.* The indicated NCI-H1299 cells were infected with VSV-GFP, SeV-GFP or Influenza-GFP at an MOI of 0.25 for 24h hours (VSV-GFP and SeV-GFP) and MOI of 1 for 24 hours (IAV-GFP), respectively. Cells were then fixed and were examined for GFP positivity to measure the percentage of cells infected using flow cytometry. Results shown are representative of at least three independent experiments, each performed with triplicate samples. Bars show the % infection of each viral strain ±SD. All assays in this figure were done in triplicate, on three biological replicates. n.s : non-significant *$p<0.05$, **$p<0.01$, ***$p<0.001$, ****$p<0.0001$. (one-side unpaired t-test).

B. NCI-H522 cells were stimulated with 1000u/mL human IFNβ1 for time point intervals and their lysates were probed with the indicated antibodies. The results confirm the endocytosis of exogenous IFNβ1 in these cells.

A

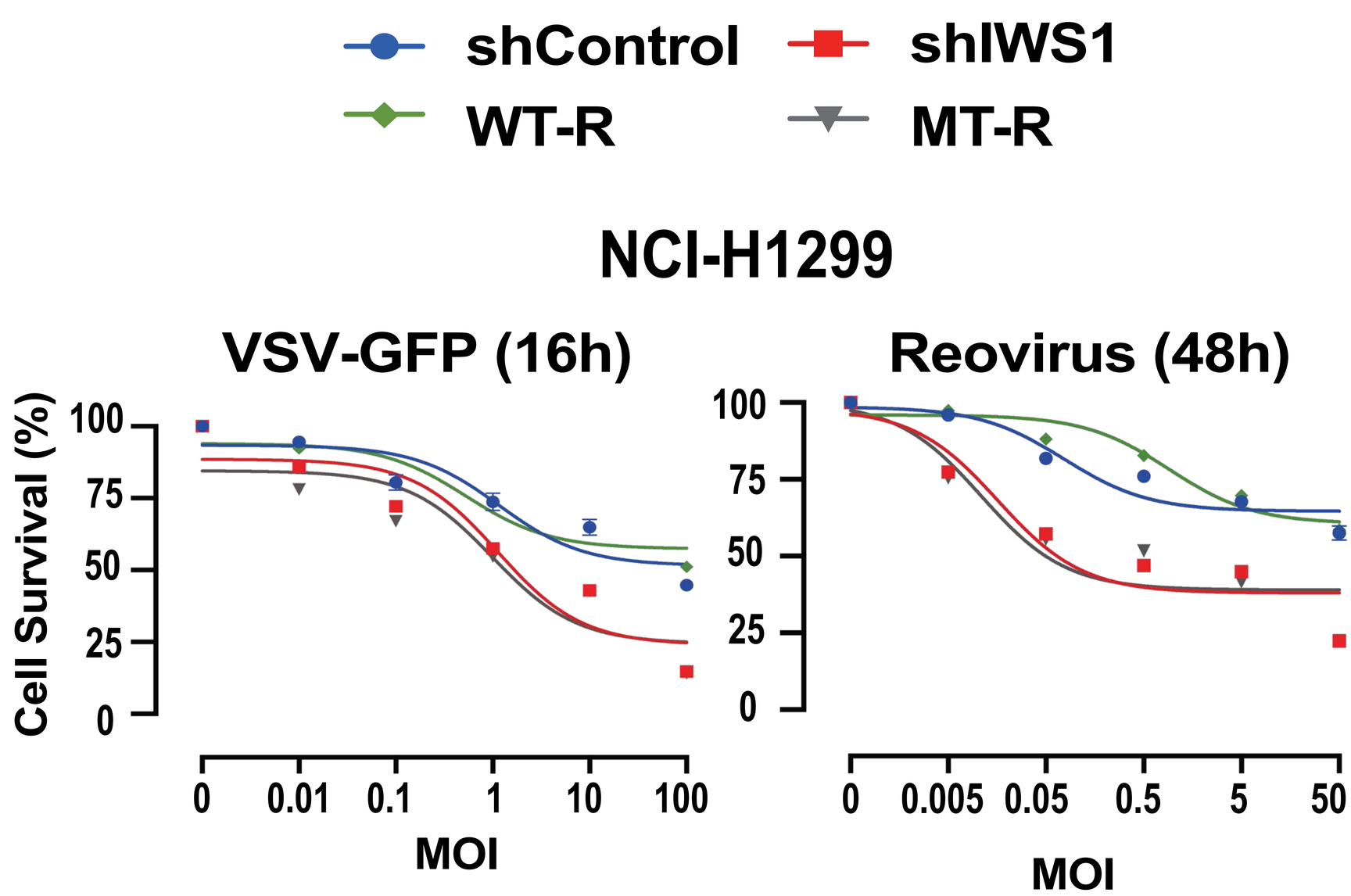
shControl
shIWS1
WT-R
MT-R
NCI-H1299
VSV-GFP (16h)
Reovirus (48h)
Cell Survival (%)
100
75
50
25
0
0
0.01
0.1
1
10
100
MOI
0
0.005
0.05
0.5
5
50
MOI

B

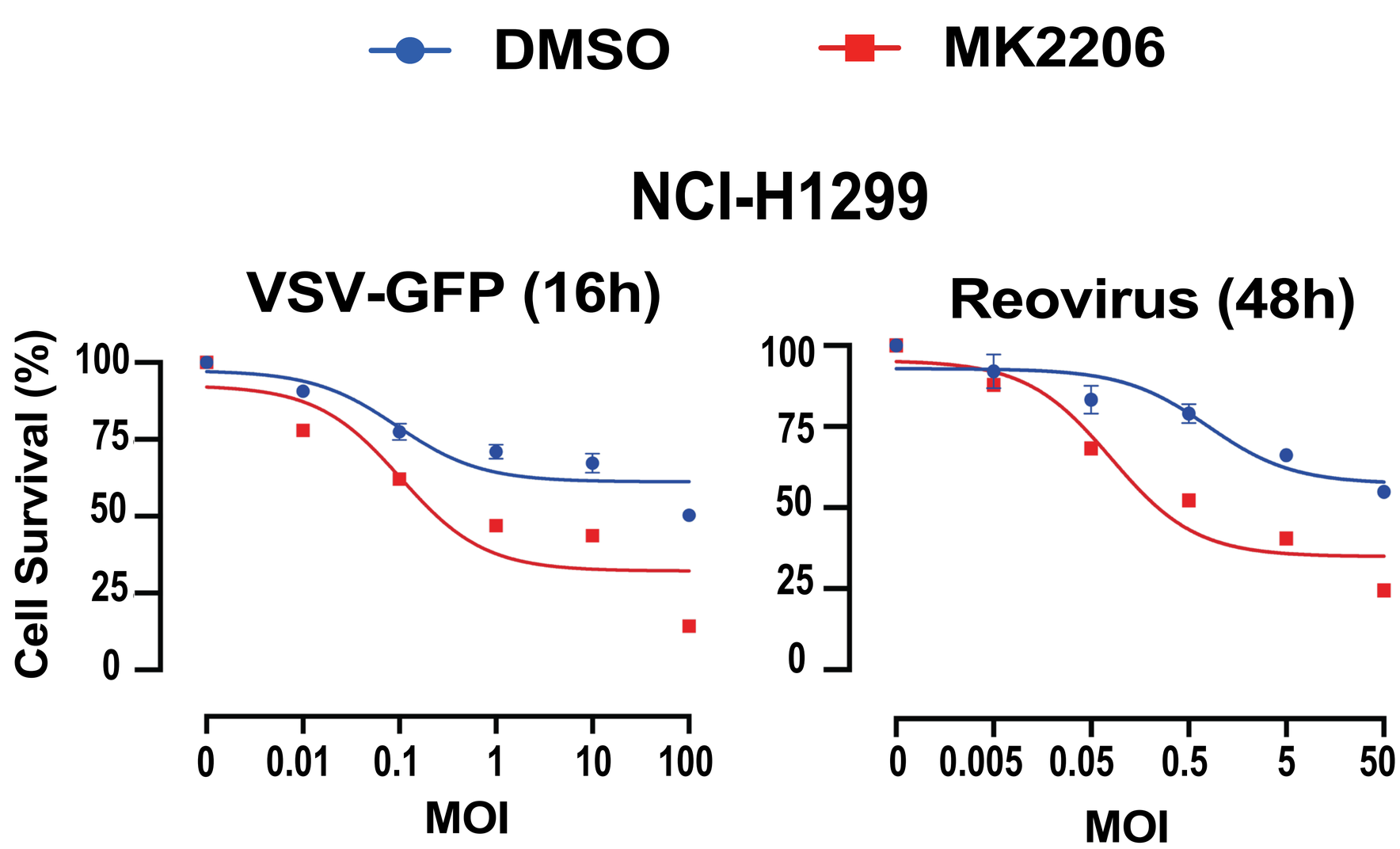
DMSO
MK2206
NCI-H1299
VSV-GFP (16h)
Reovirus (48h)
Cell Survival (%)
100
75
50
25
0
0
0.01
0.1
1
10
100
MOI
0
0.005
0.05
0.5
5
50
MOI

C

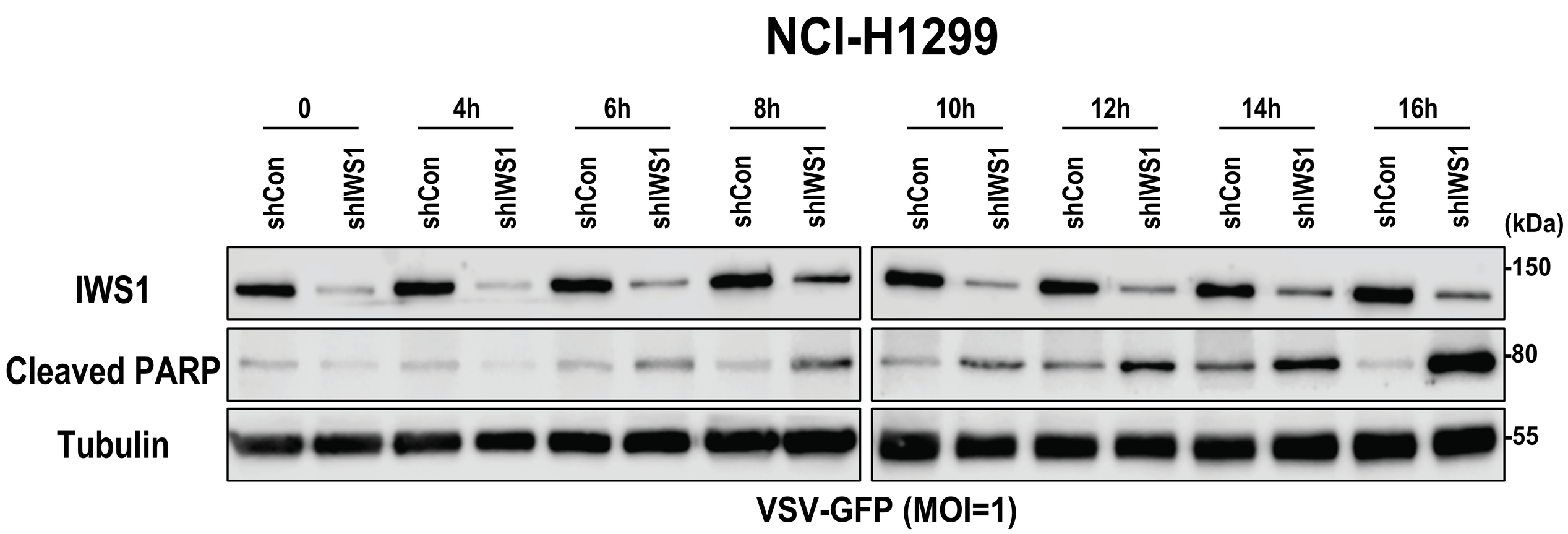
NCI-H1299
0
4h
6h
8h
10h
12h
14h
16h
shCon
shIWS1
(kDa)
IWS1
Cleaved PARP
Tubulin
150
80
55
VSV-GFP (MOI=1)

Figure S7 (Relative to Figure 7). Inhibition of the AKT/p-IWS1 axis sensitizes lung adenocarcinoma cells to oncolytic viral killing.

A. *The loss of IWS1 phosphorylation sensitizes lung adenocarcinoma cells to oncolytic viral killing.* NCI-H1299 cells transduced with the indicated constructs were exposed to increasing MOI of VSV-GFP or Reovirus for 16h and 48h, respectively. Cell proliferation was assessed by fluorescent detection of the reduction of resazurin to resorufin by viable cells and expressed as a percentage of uninfected cells. Mean values are shown ±SD (n=3), data are representative of two independent experiments.

B. *The loss of AKT/p-IWS1 axis sensitizes lung adenocarcinoma cells to oncolytic viral killing.* NCI-H1299 cells treated with DMSO or 5μM of the pan-AKT inhibitor MK2206, were exposed to increasing MOI of VSV-GFP or Reovirus for 16h and 48h, respectively. Cell proliferation was assessed by fluorescent detection of the reduction of resazurin to resorufin by viable cells and expressed as a percentage of uninfected cells. Mean values are shown ±SD (n=3), data are representative of two independent experiments.

C. *The loss of IWS1 phosphorylation sensitizes lung adenocarcinoma cells to oncolytic viral killing via Caspase-mediated death.* NCI-H1299 shControl and shIWS1 cells were infected for the indicated time point intervals with VSV-GFP at a MOI=1. Western blot lysates from these time points were probed with the indicated antibodies, showing a robust cleavage of PARP, a sensitive marker of Caspase mediated apoptosis, in shIWS1 cells even in early time points of infections.